Furnace tests on unprotected and protected concrete filled hollow structural hollow sections

Furnace tests on unprotected and protected concrete filled structural hollow sections

David Rush[1]*, Luke Bisby[1], Martin Gillie[2], Allan Jowsey[3] and Barbara Lane[4]

[1] BRE Centre for Fire Safety Engineering, University of Edinburgh, UK
[2] School of Mechanical, aerospace and Civil Engineering, University of Manchester, UK
[3]International Paint Ltd, AkzoNobel, Newcastle, UK
[4] Arup, London, UK

Abstract: The accurate prediction of cross-sectional temperatures within concrete filled steel hollow (CFS) sections is critical for the accurate prediction of fire resistance. Whilst there have been many thermal and structural tests conducted on CFS columns, there are few that report the full cross-sectional thermal profile, and when they are reported, the sensor density is low, hindering the ability to validate models. This paper presents furnace tests and thermal modelling on 14 unprotected and 20 protected CFS sections, and examines the effect of several parameters on cross-sectional thermal profiles, as well as assessing the accuracy of both Eurocode thermal analysis guidance and intumescent fire protection design guidance. This paper shows that; (a) the assumptions within the Eurocode guidance can lead to large over-estimations in cross-sectional temperatures; (b) proposes new thermal modelling assumptions in three key areas; and (c) shows that the current intumescent fire protection design guidance is very conservative.

Keywords: Concrete filled hollow sections, intumescent fire protection, furnace tests, heat transfer, thermal modelling, interface gap evolution

1 Introduction

Architects and engineers increasingly specify concrete filled steel hollow structural sections (CFS) in the design and construction of multi-storey buildings. CFS sections consist of hollow steel sections that are in-filled with concrete to provide superior load carrying capacity and structural fire resistance as compared with unfilled steel tubes. They are an attractive and efficient means by which to design and construct compressive members in highly optimized structural frames. The

* Corresponding Author. e-mail address: d.rush@ed.ac.uk, Phone number: +44 (0)131 650 7241, Address: John Muir Building, Room 1.5, BRE Centre for Fire Safety Engineering, University of Edinburgh, Kings Buildings, Mayfield Road, Edinburgh, UK, EH9 3JL.

concrete infill and the steel tube work together, at both ambient temperatures and during fire; the steel tube acts as stay-in-place formwork during casting of the concrete, thus reducing forming and stripping costs, and provides a smooth, rugged, architectural surface finish; the concrete infill enhances the steel tube's resistance to local buckling; and the steel tube sheds axial load to the concrete core when heated during a fire, thus enhancing the fire resistance of the column [1].

Multi-storey buildings may require structural fire resistance ratings of two hours or more [2] that CFS sections can often provide without the need for applied fire protection. However, when a structural fire resistance assessment [i.e 1, 3-6] shows that adequate fire resistance is unachievable without insulation, external fire protection must be applied (in the UK the preferred method of fire protection is often by intumescent coatings).

The structural performance of CFS sections fundamentally depends on the temperatures that the steel tube, internal steel reinforcement (when present) and concrete core experience during fire and after cooling [7]. Prediction of internal temperatures is thus critical to determine the amount and effectiveness of protection needed to achieve a given fire resistance. There is, however, a paucity of detailed thermal data from standard furnace tests available in the literature for both protected and unprotected CFS sections in fire. A global review of structural furnace tests [8] showed that of the 300+ available tests, only 75 included protection; 24 of these were protected with intumescent coatings and only 18 of these were tested within the past 20 years.

Furnace tests on unprotected CFS columns reported in the literature rarely report detailed cross-sectional temperatures, and there are no data available on performance during the cooling phase. Test reports that do include full temperature profiles typically have inadequate sensor density; for example tests presented in [8] and [9] measured only one steel and two concrete temperatures for each specimen, hindering their use for model validation.

Various attempts at thermal model validations have been presented previously in the literature. For example, Tao and Ghannam [11] used data from available standard furnace tests to predict the temperature profiles within CFS sections using a finite element model and suggested

possible improvements over the Eurocode's [4] prescribed modelling approaches. However, Tao and Ghannam also noted that the variable emissivity of the steel tube, the moisture content of the infill concrete, and the gap conductance at the steel tube-concrete core interface played potentially important roles in the heat transfer in CFS columns. Han et al. [12] presented and modelled the temperature profiles within unprotected and protected CFS columns during 12 furnace tests, although again the density of temperature measurement was low. These tests demonstrated that the spray applied passive fire protection materials used were effective at preventing heat transfer; they also demonstrated that it was possible to predict the steel tube temperatures of the protected CFS sections with reasonable accuracy. However, predicting temperatures in CFS sections protected with intumescent coatings continues to prove difficult [12] due to the chemical and physical changes they undergo during heating, foaming, and charring [13].

To increase the available data on protected CFS columns under standard fire testing, this paper presents results and analysis of 34 unloaded furnace tests on both unprotected and protected CFS columns of various shapes and sizes, providing temperature data throughout the heating and cooling phases of standard fire exposure. These data will allow thermal modelling approaches to be created and verified, and aims to demonstrate an ability to credibly predict the performance of CFS sections with intumescent fire protection.

2 Furnace Tests

The furnace test program was carried out in ceramic lined standard fire testing furnaces at International Paint Ltd, Newcastle. A total of 34 specimens were tested; 14 were unprotected CFS sections and 20 were protected with intumescent paint, designed in accordance with BS EN 13381-6 [14] unless otherwise stated.

2.1 Experimental Programme

The experimental programme is outlined in Table 1 and was developed to examine the influence of several parameters on the heat transfer within the sections, including: the shape and size of the sections, the steel wall thickness, the type of concrete infill, the type (severity and duration) of

thermal exposure, and the specific type of fire protection. These six parameters are used in Table 1 to identify the individual tests using the naming scheme outlined in Figure 1, with the majority of protected specimens having an unprotected counterpart for comparison. Four additional tests were performed, identified in Table 1 by ".xxx", to assess the effects of concrete age and protection thicknesses on thermal response.

Two section shapes were included: circular and square. A greater number of circular sections were tested since there are less data in the literature for circular sections, despite their popularity with architects and engineers due to their aesthetics and structural benefits (i.e. confinement of concrete core). Square sections included 300 × 300 mm and 120 × 120 mm cross-section columns, while circular sections included 323.9 mm Ø, 219.1 mm Ø and 139.7 mm Ø. Three wall thicknesses (5, 8 and 10 mm) were included, and the length of the columns was 1.4 m (except for the 323.9 mm Ø mm and 300 × 300 mm sections where the length was 1.0 m due to weight restrictions in the furnaces). It is noteworthy that 1.0 m is the minimum permissible section length according to testing standards for intumescent paint on CFS sections [14]. All tubes were made from Grade S355 steel (355MPa nominal yield strength).

The concrete infill used was a ready-mix, high strength, hybrid steel and polypropylene (PP) fibre reinforced mix (FIB), at 45 kg/m^3 and 2 kg/m^3, respectively. The cement paste contained 31.5% of silica fume and blast furnace slag combined with Portland cement, whilst the aggregate was basalt. Two specimens (C-1-1-H-I-N and C-1-1-H-I-C1) were filled with high strength concrete (HSC) using the same mix design as the FIB concrete mix but without steel or PP fibres. The test day strengths of the FIB and HSC concrete mixes were between 47 - 59 MPa and 48 MPa, respectively, whilst the moisture content was between 3.4 - 4.9% and 3.0% by mass, respectively fr. Specimens were cured for at least 6 months after casting before testing. Exceptions were tests C-1-1-F-I-C1.14d and C-1-1-F-I-C1.28d, which were cured for 14 and 28 days, respectively, to assess the effect of concrete age, on the heat transfer within the sections; which informed the development of testing standards [14] for fire protection of CFS sections.

Two thermal regimes were used: ISO 834 [15] standard fire exposure and the Eurocode slow growth smouldering curve [16]. These were selected to advance understanding of the heat transfer in CFS sections, particularly as regards the performance of intumescents under non ISO 834 heating regimes.

2.2 Fire Protection Design

Design of intumescent fire protection systems applied to structural steel is typically based on: (1) the required *fire resistance* (FR), which is typically prescribed by local building codes (e.g. [2]); (2) a *section factor,* defined as the ratio of the section's heated perimeter, H_p, to its cross sectional area, A; and (3) an assumed steel *limiting temperature*, which is the temperature at which the steel is presumed to fail under load during a standard furnace test, and which may depend on the structural element's *utilisation* during fire. Engineers use these three parameters, in conjunction with empirical product specific design tables, to specify the required dry film thickness (DFT) of the intumescent needed to maintain the temperature of the steel below the limiting temperature for the required duration of fire. Product specific design tables for intumescents are based on numerous large-scale furnace tests on structural steel sections with various section factors and applied DFTs.

To apply existing DFT tables developed for open or unfilled steel sections for protection to CFS sections, an 'effective' section factor, H_p/A_{eff}, is needed to take account of the effect(s) of the concrete infill on the heating rates of the steel. Equations 1 and 2 represent the current approach to determining the effective section factor for CFS sections [17] in the UK. These equations treat the problem by applying DFT design guidance developed for unfilled steel sections but adding an 'equivalent' steel wall thickness, $t_{c,e}$ (in mm), which is dependent on the internal breadth of the section, b_i (mm) and the required fire resistance time, t_{FR} (mins), to the existing steel wall thickness, t_a (mm), to account for the thermal effect of the concrete core, thus decreasing the effective H_p/A:

$$\frac{H_p}{A_{eff}} = \frac{1000}{t_a + t_{c,e}} \quad (1)$$

$$t_{c,e} = \begin{cases} 0.15b_i, & b_i < 12\sqrt{t_{FR}} \\ 1.8\sqrt{t_{FR}}, & b_i \geq 12\sqrt{t_{FR}} \end{cases} \quad (2)$$

It should be noted that neither the theoretical or empirical rationale for these equations are reported in the literature. Nonetheless, whilst the approach seems physically unrealistic and potentially flawed on various grounds, it is the approach used on real projects.

Equations 1 and 2 were used to prescribe the intumescent coating DFTs for the protected CFS sections presented in Table 1. These are based on an FR time of 90 minutes and a limiting temperature of 520°C in the steel tube under ISO 834 heating. Exceptions were columns C-1-1-F-I-C1.120 and C-1-1-F-I-C1.75, which had DFTs based on FR times of 120 and 75 minutes, respectively, again with a limiting temperature of 520 °C.

It should be noted that the concept of a steel limiting temperature is not strictly applicable to CFS columns due to the presence of the concrete in-fill within the CFS section. For unfilled steel sections, designers are able to rationally calculate accurate limiting temperatures based on the applied load level (i.e. utilisation) during fire [18]. However, CFS sections experience a complex heating-rate-dependent thermal gradient within their concrete core, due to the presence of the load carrying concrete infill, and thus the calculation of the limiting steel temperature for CFS sections is considerably more complex. Calculating the appropriate steel limiting steel tube temperature is inherently iterative as it is a product of itself, the size of the section, the required FR time, and the specific fire protection system being used. Additional discussion and information on this issue has been presented by Rush et al. [19]; however it should be noted that it remains common in practice to assume a steel limiting temperature 520°C (or 550°C) to design intumescent DFTs for CFS sections, and this thus used herein.

Fire protection was achieved using two commercially available intumescent fire protection coatings at two thicknesses, as outlined in Table 1. These were supplied by an industry partner (International Paint, UK). Coating 1 (C1) was Interchar 1120*; a water-borne, single pack (i.e. one

* Specific trade names are provided purely for the purposes of factual accuracy.

component) thin film intumescent coating; and Coating 2 (C2) was Interchar 212*; a two pack intumescent epoxy coating. This allowed an initial assessment of the response of different types of intumescent coatings on CFS sections.

2.3 Specimen Preparation and Test Procedures

The steel tubes incorporated vent holes and lifting holes to allow vapour pressure to escape during heating and also to enable easy handling. A schematic of the test specimens is given in Figure 2. Temperature readings were taken at two heights ($L/3$ and $2L/3$) using Inconel sheathed K-Type thermocouples (TCs) [14], [20]. Figure 2 shows the typical TC layouts at each height: four TCs measured mid-thickness steel tube temperatures; four measured the concrete temperatures at the steel-concrete boundary (denoted "Conc. face TC"), nominally 2.5 mm from the steel surface; two were placed 35mm from the concrete-steel interface; and one was placed at the centreline of the cross-section. All TC wires were routed internally so as not to interfere with the reaction of the intumescent coating. For the circular sections external steel TCs were evenly spaced around the circumference, whilst for square sections pairs of TCs were placed opposite each other either mid-wall or at the corners.

After TC placement, the steel tubes were filled with concrete and allowed to cure for at least six months, after which the protected specimens were coated with the relevant intumescent coating and thickness, as outlined in Table 1. Casting of C-1-x-x-x-x sections was hampered by the TC wires and support structures that ran internally within the tubes; these impeded the flow of the concrete into the tubes. Considerable rod vibration was required to ensure that the tubes were full, potentially dislodging or damaging TCs. The intumescent coatings were applied according to the manufacturer's specifications, including minimum cure times between coatings; for coating C1 five layers (six layers for C-1-1-F-I-C1.120, four layers for C-1-1-F-I-C1.75) were required to reach the required DFT, with 24 hours cure time required between each layer of application. Coating C2 was applied in a single layer. After the required DFTs had been applied, the specimens were left to cure

for at least seven days to fully cure (apart from C-1-1-F-I-C1.14d which only had three days at full DFT to cure due to time constraints).

All specimens protected to 75 or 90 minutes were heated for 120 minutes, except specimen C-1-1-F-I-C1.120, which was protected to 120 minutes, and was heated for 180 minutes. The specimens were heated for 120 minutes or more as FRs of 120 minutes or more are often needed in high-rise applications. After 120 minutes of heating (or 180 minutes for C-1-1-F-I-C1.120), the gas supply was halted and data were recorded for a further two hours during cooling. All specimens were tested unloaded.

A 1.5 × 1.5 × 1.8 m^3 testing furnace was used for the tests at 14 and 28 days (C-1-1-F-I-C1.14D and C-1-1-F-I-C1.28D), the smouldering fire tests (x-x-x-x-S-x), and the tests with variable design fire resistance (C-1-1-F-I-C1.120 and C-1-1-F-I-C1.75). A 4.0 × 3.0 × 2.0 m^3 furnace was used for all other tests due to a change of testing facilities by the industry partner. Both furnaces were lined with ceramic tiles, and ceramic wool was placed over the tops and the base plates of the specimens to provide idealized two-dimensional heat transfer within the specimens' cross-sections. Furnace temperatures were controlled using the same K-Type thermocouples in accordance with BS 476 [21].

3 Unprotected CFS Sections

Application of fire protection to CFS columns can be expensive and time consuming, and there is therefore a desire to use CFS columns without protection provided this can be done safely. To predict the structural capacity of an unprotected CFS column during fire, accurate predictions of cross-sectional temperatures are an essential prerequisite. In this section the 14 tests on unprotected CFS sections are compared against thermal predictions made using the best available guidance.

3.1 Temperature Predictions in Unprotected Specimens

Cross-sectional temperatures within the unprotected CFS sections were predicted using Eurocode guidance [4, 16]. A two-dimensional heat transfer mesh, shown in Figure 3, was divided into 4 element regions; region D represents the steel tube; region C represents the initial 5 mm of concrete;

region B represents the subsequent 30 mm of concrete; and region A the remaining concrete core to the centre of the cross-section. The mesh employed 4-noded heat transfer elements (apart from a single ring of triangular elements near centre for circular sections), using 9/8/4/4 elements in the regions A/B/C/D, respectively, for the x-1-x-x-x-N sections and 17/8/4/4 for all other sections. A sensitivity analysis confirmed the suitability of the chosen mesh density [22].

Guidance is given in Eurocode 1 [16] for predicting heat transfer from a testing furnace environment to test assemblies. The net heat flux, $\dot{h}_{net}$, is calculated based on convective and radiative heat transfer, according to:

$$\dot{h}_{net} = \left[\alpha_c \cdot \left(\theta_g - \theta_m\right)\right] + \left[\Phi \cdot \varepsilon_m \cdot \varepsilon_f \cdot \sigma \cdot \left[(\theta_r + 273)^4 - (\theta_m + 273)^4\right]\right] \quad (3)$$

where the emissivity of the fire is taken as $\varepsilon_f = 1.0$, the emissivity of the steel is $\varepsilon_m = 0.7$, the view factor is assumed as $\Phi = 1$, and the convective heat transfer coefficient is taken as constant at $\alpha_c = 25\ \mathrm{W/m^{2}{\cdot}^{\circ}C}$ for heating in accordance with ISO 834; θ_m is the temperature of the material, θ_g is the gas temperature, and θ_r is the radiative temperature of the fire, which may be assumed to be equal to θ_g for members in a furnace [16].

Eurocode 4 [4] suggests thermal properties for steel and concrete; these are not reproduced here but include the variation in density, $\rho_{i,\theta}$, thermal conductivity, $\lambda_{i,\theta}$, and specific heat capacity, $c_{i,\theta}$, for both steel and concrete. An *Eurocode* prediction modelling exercise was performed assuming 10% water content in the concrete and the 'lower bound' thermal conductivity curve from Eurocode [4]. It should be noted that the Eurocode guidance [4] assumes perfect contact between the steel tube and concrete core, despite the fact that previous furnace tests on CFS columns have shown the formation of a gap due to differential expansion between the steel tube and the infill concrete. No direct research has been performed to understand gap formation, although limited research has been undertaken to study its possible thermal effects [23], [24].

Predicted temperatures at 30, 90 and 120 minutes are given in Table 2. Single temperature values are given at the specific time and location for circular columns, due to axisymmetric heating

of the cross-sections, whereas mid-wall and corner temperatures (shown in brackets) are given for the square sections in which the heat transfer is two-dimensional.

3.2 Results and Observations: Unprotected Tests

Selected results of the unprotected tests are presented in Table 3. Temperatures averaged across all TCs at a given location are given at 30, 90, and 120 minutes, as are the maximum temperatures and the times they were reached. In general it appeared that the aforementioned concrete consolidation problems during casting had little effect on observed temperatures. However, specimen C-1-2-F-I-N had incomplete data from four of the six concrete 35mm and centreline thermocouples whilst C-1-3-F-I-N displayed a great deal of variability at the concrete face and centreline TC locations, where temperatures varied by up to 210^{o}C and 110^{o}C, compared to variability in most other sections of 80^{o}C and 10^{o}C. These measurements were not included in the subsequent comparisons.

Representative temperatures within a circular CFS column (C-2-2-F-I-N) under an ISO 834 fire are shown in Figure 4. The maximum temperature in the steel tube occurred at 120 minutes in all cases. The observed concrete face temperatures followed a similar trend to those measured in the steel tube; also with lower temperatures again peaking at 120 minutes. The lower temperatures observed at the surface of the concrete are a result of the thermal resistance at the interface between the steel tube and the concrete infill (possibly influenced by the formation of an air gap during heating) and to possible mis-placement of the thermocouples at this location (discussed below). The vaporisation of free water has a clear retarding effect on temperatures observed in the concrete between 120 and 200^{o}C.

Also presented in Figure 4 are the predicted temperatures in C-2-2-F-I-N, showing that using the *Eurocode* thermal modelling approach predictions of temperature are relatively poor; temperatures in the steel and close to the concrete surface are over-predicted while temperatures toward the centre are slightly under-predicted, due to the model; a) over-predicting the heat transfer from the furnace to the steel; b) presuming perfect contact at the steel-concrete interface; and c) over-estimating the thermal properties of the concrete (namely moisture content and thermal

conductivity). These trends hold for all the unprotected specimens tested. For example, Figure 5 shows the average prediction errors for all unprotected sections exposed to an ISO-834 fire, for the steel, concrete face and concrete centre TC locations.

The prediction errors in Figure 5 are believed to be due to inappropriate thermal modelling assumptions rather than caused by TC misplacement, since the data set represents average temperatures. This is confirmed by Figure 6, which shows that a TC misplacement error of ±2.5 mm is effectively insignificant apart from at the concrete face where misplacement errors of 140^{o}C are possible.

Cross-sectional Effects on Temperatures

The observed temperatures observed were influenced by the size and shape of the cross-section, as shown in Figure 7 and 8. Figure 7 shows steel tube temperatures for circular and square sections, respectively, and suggests that as the size of the cross-section increases the temperatures in the steel decrease. For example, the reduction in steel temperature between C-1-x-F-I-N and C-3-x-F-I-N sections was about 80^{o}C at 120 minutes. Steel temperatures increased slightly within each section size as the wall thickness increased (refer to Table 3), with maximum steel temperatures typically observed for 10 mm wall thickness. The physical reasons for this are not known. Square cross-sections experienced higher temperatures at the corners, as expected, than at the middle of the steel tube wall, due to the increased surface area at the corners.

Figure 8 shows that as the section size increased the temperatures at the concrete face decreased due to increased thermal mass of the larger cores. For instance, at 120 minutes the temperature difference between C-1-x-F-I-N and C-3-x-F-I-N sections was approximately 140^{o}C. The concrete face temperatures for S-1-x-F-I-N sections showed similar differences between mid-wall (M.W.) and corner (Corn.) temperatures as for steel tube temperatures (Figure 7). This was not the case for S-3-3-F-I-N, in which the concrete face mid-wall temperatures were much lower (by 150^{o}C) than those seen at the corner in the steel tube. This is possibly due the thermal conductivity of concrete being low compared to steel; thus after an air gap has formed less heat is transferred

through conduction and the temperature difference between the mid-point of the face to the corner increases in the concrete.

Figure 8 shows that concrete centreline maximum temperatures occurred 15 minutes after the end of heating for S-1-x-F-I-N and C-1-x-x-I-N sections, with values approximately 100ºC lower than the maximum concrete face temperatures observed at 120 minutes of heating. In C-2-x-F-I-N, C-3-x-F-I-N and S-3-3-F-I-N sections maximum temperatures were lower and peaked later, after the maximum gas temperature, due to the increased thermal mass of the cross-sections. The thermal mass of the concrete core is particularly affected by the energy consumed in evaporating free water between 120 and 200ºC; this was clearly observed in all concrete centreline TC measurements (Figure 8). Larger sections had larger volumes of free water available for vaporisation, which resulted in lower and later maximum temperatures. This is important as it demonstrates that the temperatures experienced during the heating phase of a CFS column may not result in the weakest condition of the concrete core, and failure of a CFS column could thus occur after a fire has been extinguished, particularly for larger columns.

Air Gap Formation

Figure 5 shows that temperature prediction errors for the concrete face are generally greater than for the steel tube temperatures. This may indicate that an air gap forms at this interface (as widely stated in the available literature [5]) and that this may affect the heat transfer. This is highlighted by observing the temperature differential at the interface between the steel tube and the concrete face, $\Delta\theta_{gap}$, in Figure 9. The average $\Delta\theta_{gap}$ for the unprotected circular sections during heating is given along with maximum and minimum $\Delta\theta_{gap}$ for each diameter of section. Peak $\Delta\theta_{gap}$ increases as the section size increases, although the rate of increase before peak $\Delta\theta_{gap}$ is reached is similar across the different section sizes, which could be due to the evolution of larger gap thicknesses in the C-2-x-F-I-N and C-3-x-F-I-N sections, as suggested in the literature [24].

Figure 9 also shows a sudden rate change in $\Delta\theta_{gap}$, at 8, 9, and 13 minutes for the C-3-x-F-I-N, C-2-x-F-I-N, and C-1-x-x-I-N sections, respectively. This may indicate the initiation of gap

formation due to differential thermal expansion. This is supported by the idea that the larger sections with lower average concrete temperatures, and thus a smaller degree of lateral thermal expansion in the concrete, would experience earlier separation of the steel tube.

Influence of Infill Type and Fire Exposure

Two unprotected sections were exposed to a smouldering fire curve [16] for 120 minutes to assess the thermal modelling approaches under different thermal insults. C-1-1-F-S-N and S-1-1-F-S-N exhibited similar responses to those discussed previously; however with slightly lower temperatures due to the less severe heating. When considering temperature differences at the steel-concrete interface, similar post peak gradients were observed with lower peak temperatures occurring later compared to ISO 834 heating. This is due to slower heating during the initial stages, thus reducing thermal gradients. The addition of steel and PP fibres to the concrete mix had no impact on heat transfer within the concrete.

3.3 Heat Transfer Unprotected CFS Columns in Fire

The furnace tests showed that the *Eurocode* model predicted temperatures within unprotected CFS sections were poor due to (i) inaccurate prediction of heat transfer from the furnace to the steel tube, with steel temperatures consistently over-predicted; (ii) not accounting for the impacts of the air gap which forms at the steel-concrete interface, with greater over-predictions at the concrete face than in the steel; and (iii) inaccurate heat transfer modelling within the concrete, especially in accounting for the effects of moisture. This section seeks to improve predictions of temperatures within unprotected CFS sections during furnace tests. C-2-2-F-I-N (219.1 × 8 mm Ø) is used as an exemplar.

A systematic forensic assessment of thermal properties and interactions was performed using the recorded temperatures at various locations as inputs to the thermal model and sequentially building up the complexity of the modelling. The appropriate concrete thermal properties were first determined using concrete face temperatures as inputs, followed by the appropriate steel-concrete

interface thermal properties, and lastly the appropriate steel-to-furnace environment thermal interaction. These are discussed in reverse order in the following sections.

Heat Transfer to the Steel Tube

The *Eurocode* approach specifies constant emissivity for the fire (ε_f= 1.0) and the steel tube (ε_m = 0.7) [16]. Figure 5 shows that using these two emissivities results in over-prediction of temperatures in the steel tube. Data in the literature, however, show that the emissivity of steel is temperature dependent. For instance, Paloposki and Leiedquist [25] provide data from which an approximation of the variable steel emissivity can be assumed as:

$$\varepsilon_m = \begin{cases} 0.2, & \theta_a = 20^oC \\ 0.2, & \theta_a = 385^oC \\ 0.65, & \theta_a = 550^oC \\ 0.65, & \theta_a = 1200^oC \end{cases} \quad (4)$$

When the above values are used to model heat transfer to the CFS with ε_f= 1.0, steel tube temperatures are still over-predicted by 100ºC in some cases. This implies that either the furnace emissivity is less than 1.0 in reality, or that the convective heat transfer is overestimated by the simplified Eurocode [16] procedure for dealing with convection. To match the observed temperatures from the current tests, a furnace emissivity, ε_f, of 0.38 had to be assumed, along with the variable steel emissivity assumptions given above. A furnace emissivity of 0.38 is slightly higher than the emissivity of a clean gas, i.e. between 0.2-0.3 [26], most likely due radiation from the hot furnace walls. Whilst not the focus of the current paper, is noteworthy that the furnace environment is vastly different to most real fires in which the emissivity of sooty smoke may be 0.8 or higher [26], where a greater thermal insult to the structure would be expected for the higher emissivity real fires. The shape of, and specimen layouts within, a furnace will also affect the resultant emissivity ($\varepsilon_m.\varepsilon_f$) experienced by the specimens, and great care needs to be taken in the set-up of tests and in assessing their results. Unfortunately, a quantitative assessment of the emissivity of the smaller furnace used herein cannot be made due to the lack of appropriate specimens to assess. It is recommended that further work be undertaken to inform these assumptions and

potentially to develop a numerical expression for fire emissivity based on furnace characteristics which would allow users to normalize standard test results from different furnaces.

Capturing the Effects of Air Gap Formation

As noted previously, it appears that the formation of an air gap at the steel-concrete interface, and the resulting thermal resistance, is important for capturing the heat transfer process within a CFS column in a furnace test. Eurocode methods [4] assume perfect contact between the steel tube and concrete core; this fails to accurately predict the temperature difference at this interface (see Figure 9).

As a representative example, Figure 10 shows the predicted temperature differential at the steel-concrete interface, $\Delta_{gap,\theta}$, that was measured in Section C-2-2-F-I-N, along with the predicted temperature differential obtained using the Eurocode procedures for heat transfer modelling. Also shown is the predicted temperature differential resulting from application of a gap conductance model proposed by Ghojel [23] at the steel-concrete interface; there is a marked improvement in the predicted temperature differential, with a maximum prediction errors during the heating phase of about 40ºC. Ghojel's [23] thermal conductance model (given in Equation 5) empirically accounts for the evolution of the air gap and the resulting heat transfer, and was developed from heating tests on 140 mm ∅ CFS sections with 6 mm wall thickness heated in an electric furnace. The resulting empirical correlation is:

$$h_j = 160.5 - 63.8 \cdot \exp(-339.9 \cdot \theta_s^{-1.4}) \tag{5}$$

where h_j is the thermal conductance across the gap in W/m^{2}K, and θ_s is the temperature of the steel in °C.

Whilst Ghojel's [23] thermal conductance model predicts the observed temperature differential gap for C-2-2-F-I-N, which is similar in scale to the tests upon which the gap conductance correlation is based, it does not necessarily reflect the gap conductance within CFS columns under all conditions (i.e. Equation 5 may not be applicable to sections where gaps do not form due to slow heating rates in protected sections). Additional testing is needed to fully

understand the conditions under which air gaps form for the interaction to be properly characterized and modelled.

Heat Transfer within the Concrete

The appropriate thermal properties to assume for the concrete in the core were determined by applying the measured concrete face temperatures to the outer ring of the concrete in the model (i.e. Region C in Figure 3), and then calibrating to the measured core temperatures by varying the specific heat and thermal conductivity of the concrete using informed trial and error. This is the only credible method since it is not possible to directly measure the thermal properties of concrete under transient steep thermal gradients. Figure 11 shows the observed and Eurocode predicted concrete temperatures for representative Column C-2-2-F-I-N, which shows under-prediction of the concrete temperatures and fails to capture the water vaporisation.

The Eurocode approach to account for the vaporisation of free moisture from the concrete is to include a spike in the heat capacity of concrete at temperatures at which this is presumed to occur [4]. In the current modelling exercise, to capture the observed thermal response of the moisture within the concrete, a modified concrete specific heat capacity model is proposed that seeks to have the same area under the heat capacity curve as the Eurocode model, although it distributes this area over a larger temperature range. The proposed specific heat capacity model is given in Equation 6 and shown in Figure 12 for a moisture content of 6.5% by mass.

$$c_{c,\theta} = \begin{cases} 890 + 56.2(\theta_c/100) - 3.4(\theta_c/100)^2 & 20^oC \le \theta_c < 120^oC \\ 2780 & \theta_c = 127°C \\ 2580 & \theta_c = 210°C \\ 890 + 56.2(\theta_c/100) - 3.4(\theta_c/100)^2 & 220^oC \le \theta_a < 1200^oC \end{cases} \quad (6)$$

The shape of the new model is rectilinear rather than triangular since as a mass of concrete is heated, in addition to vaporisation of moisture there is also movement of moisture away from the heated face via micro-pores in the concrete. As the moisture migrates, pressure develops within the concrete and this increases the temperature at which the moisture will vaporise (in accordance with the ideal gas law). It is also assumed that the size of the pores within the concrete is non-uniform and that the moisture within the pores is at different pressures at different location, due to different

sizes of pores. Thus the moisture is assumed to evaporate at different temperatures in different locations. The assumed moisture content of 6.5% by mass is more than the 4.9% obtained by mass loss dehydration of concrete cylinders since increased moisture expected given the encasement of the concrete core in a CFS section. The moisture effect is assumed to act over a range from 120°C to 220°C based on our test data, and the proposed rectilinear shape was determined through curve fitting on representative Column C-2-2-F-I-N.

Thermal Predictions with Model Enhancements

Figure 13 shows the observed and predicted temperatures in C-2-2-F-I-N using the enhanced modelling approach. This includes the best thermal properties and interactions identified in the previous three sections; i.e. the fire emissivity is taken as 0.38 and the emissivity of steel is assumed as temperature dependent (Equation 4); Ghojel's [23] air gap thermal conductance model is included (Equation 5); and the modified specific heat model for concrete (Equation 6) is used. As expected, the enhanced model shows an improvement (compare Figure 4 and Figure 13) compared to the predictions made using the Eurocode approach for representative Column C-2-2-F-I-N. The enhanced model also shows an improvement when applied across all the unprotected sections tested. This can be seen by comparing Figure 5 and Figure 14 which shows that the steel temperatures, heat transfer at the steel-concrete interface using Equation 5, and that temperatures within the core using Equation 6, are all accurately predicted (± 50°C on average) through both the heating and cooling phases. The authors recommend incorporating equations 5 and 6 into thermal models in future design applications, and also that engineering judgment be used in determining the heat transfer to the steel tube from a real fire.

4 Protected CFS Sections

Intumescent paint is the predominant form of fire protection for structural steel in the UK. There is, however, a paucity of fire test data on CFS sections protected with these materials. Available design guidance for the application of intumescent coatings is necessarily conservative given the paucity of data, and can result in costly fire protection solutions. To begin to address this issue, a further 20

furnace tests were performed on protected CFS specimens, as outlined in Table 1. The aim was to better understand the performance of intumescents when applied to CFS sections and to improve design guidance for specifying and optimising the coating thickness.

4.1 Temperature Predictions in Protected Specimens

The dry film thickness (DFT) of intumescent for the tests was selected (in all but two cases) using available UK guidance (described earlier) assuming a limiting steel temperature of 520^{o}C after 90 minutes of fire exposure to the ISO 834 [15] standard fire. The temperature of 520^{o}C is deemed by the UK to be a conservative limiting steel temperature for a structural hollow section (i.e. unfilled) acting in compression, derived in accordance with BS 5950-8 [27] for typical worst-case loading in the built environment. Historically, passive fire protection thickness tables have been presented with respect to this temperature. It should be noted that a similar exercise to define a limiting temperature in accordance with the Eurocodes and the UK National Annex resulted in a temperature of 515°C [28]. Predicting temperatures in protected sections, other than the steel tube temperatures of 520^{o}C at 90 minutes of exposure is outside the scope of this paper as it involves understanding of modelling the complex thermal and physical evolution of intumescent chars during heating [29].

4.2 Results and Observations: Protected specimens

Table 4 shows selected temperatures measured in protected CFS sections during fire testing at various TC locations, after 30, 90, and 120 minutes of exposure, as well as the observed maximum temperatures and times at which these occurred. Temperatures within protected sections were significantly lower than those observed in the unprotected tests, as expected, clearly confirming the effectiveness of the protective coatings for fire durations exceeding 120 minutes. For example, Table 4 shows that only two of the protected sections (C-1-1-F-I-C1.75 and C-1-1-F-I-C1.120) actually reached the limiting steel temperature of 520^{o}C during heating, and in both cases this occurred more than 30 minutes *after* the as-designed fire resistance time.

The peak steel temperatures in C-1-1-x-x-C1 sections occurred at about 180 minutes, compared with 120 minutes in all other sections, this is due to the gas extraction in the furnace

being turned off coincident with the gas supply in these tests, whereas in the other tests the gas extraction remained on resulting in rapid cooling. It should be noted that the char layer not only prevented heating of the specimens during fire but also slowed their cooling; in practice this could affect CFS columns' post-fire residual capacity, since the longer concrete is at temperatures above 300^{o}C the greater the damage suffered [30].

It is noteworthy that sections x-1-1-F-S-C1, C-1-1-F-I-C1.xxD, and C-1-1-F-I-C1.xxx were tested in a smaller furnace as compared with all other tests. Analysis of the data demonstrated that distinct differences existed in the thermal responses to the same imposed temperature-time curve in the respective furnaces; the smaller furnace produced considerably higher specimen temperatures for similar CFS sections despite identical gas phase temperatures. For instance, comparison of C-1-1-F-I-C1 and C-1-1-F-I-C1.28D show that temperatures recorded in the steel tube at 120 minutes were 458^{o}C and 366^{o}C, respectively. While the reasons for this are complex and not well understood, and in any case this issue is not the focus of the current paper, it is recommended that additional research on heat transfer in standard fire testing furnaces be carried out so that predictions of heat transfer to specimens in "controlled" furnace environments can be accurately made [31].

The char integrity in most tests was excellent, however in two tests (S-1-1-F-S-C1 and C-2-2-F-I-C1) longitudinal splitting of the char was observed, as shown in Figure 15 (c) for the C-2-2-F-I-C1 specimen. This allowed localised heating of the steel tube and slightly raised the recorded temperatures. Figure 16 shows temperatures in C-2-2-F-I-C1 and suggests that local splitting of the coating only slightly affected the overall temperatures; steel tube and concrete surface temperatures in the vicinity of the split are shown along with average temperatures at each location (excluding the temperatures adjacent to the split). For a column in a real building, one might expect more cracking to occur in the char for these columns due to the influence of local restraint forces from the surrounding structural frame; however as seen in the tests, the influence on cross-sectional temperatures would be expected to be minimal and localised.

Steel Tube Temperatures

Two different specific intumescent coatings were studied in the current testing programme. Coating C1 began to react at temperatures of about 100ºC, as shown in Figure 17. A steep initial increase was apparent in steel temperatures during the initial 10 minutes of heating followed by a drastically reduced rate once the coating had activated. Coating C2 displayed reduced heating rates in the range of approximately 180ºC in the steel. This was expected based on data provided by the fire protection supplier.

Figure 17 shows that the steel temperatures after 90 minutes were considerably lower than the design temperature of 520ºC (these were between about 180-250ºC for all columns with Coating C1). The steel temperatures with Coating C2 were between 170-250ºC higher after 120 minutes than their C1 coated counterparts, however still well below the design limiting temperature of 520ºC. It is clear that the available design guidance used to select DFTs for CFS columns is highly conservative for the products and sections tested herein.

The trends observed in the unprotected tests were also evident for the protected tests. Steel temperatures increased as the section size decreased; corner temperatures of square specimens were higher than at the mid-wall; and mid-wall square section temperatures were equivalent to the temperatures observed in the steel of the circular sections with equivalent heated perimeter to total cross-sectional area ratios, all as expected

Concrete Temperatures

Temperatures at the concrete face in the protected sections were similar to those in the steel tube due to the insulating effects of the coating. The temperature differential at the steel-concrete interface for the protected sections were thus significantly lower (Figure 18) than those observed in equivalent unprotected tests (Figure 9). The temperature difference at the steel-concrete interface in the protected cases remained constant after the intumescent reacted, with temperature differences less than 50ºC or 100ºC for the C1 and C2 coatings, respectively. One exception is in the region near the split in the coating for C-2-2-F-I-C1, where the temperature differences increased

dramatically to levels similar to those seen in the unprotected tests. The smaller temperature differences observed at the steel-concrete interface suggests that gap formation was less pronounced (or did not occur) at the slower heating rates. The higher temperature differences experienced for the C2 coating were due to the higher intumecent reaction initiation temperature required for this coating, and perhaps the formation of a small air gap.

The concrete TCs showed the same overall response in the protected tests as in the unprotected tests, with plateaus in temperature between 100 and 180ºC indicating vaporisation of moisture from the concrete (Figure 19). Concrete centreline temperatures in x-3-x-x-x-x sections continued to increase after 240 minutes, and similar temperatures were seen in sections with similar heated perimeter to total cross-sectional areas (i.e. x-3-x-F-I-Cx and x-1-x-x-I-Cx sections). C-1-x-x-x-C1 sections showed considerable variation, similar to that seen previously for the unprotected sections (Table 3), and for the same reasons.

Influence of Fire Exposure

Safe design and application of reactive coatings on CFS columns requires that the coatings be assessed under different credible fire exposures to ensure that sufficient/consistent thermal protection is observed under non-standard heating. This is particularly important for performance-based designs where design fires may be specific to the particular design. The observed temperatures in specimens exposed to the smouldering curve were similar to those recorded in tests under the ISO 834 standard fire curve; this is surprising given that the smouldering curve specifies lower temperatures throughout. This may be due to the fact that different furnaces were used in the smouldering tests (i.e. the smouldering tests used the smaller furnaces which appeared to exert a more severe thermal insult for the reasons discussed previously).

The intumescent char split at about 75 minutes on S-1-1-F-S-C1, locally increasing the steel tube temperature; however, the average temperature of the steel remained below 520ºC (Table 4). Similar thermal responses were observed within the concrete as for the unprotected tests; although with markedly lower temperatures.

Influence of Concrete Age and Protection Thickness

Current certification practices within the reactive coating industry require intumescent coating suppliers who wish to apply their products on CFS sections to perform furnace tests to demonstrate adequate performance [20]. Within the industry there is currently some question as to the required duration of concrete core curing to allow the concrete to cure to such an extent that a 'realistic' thermal response is observed, given that the thermal response is presumed to depend to some extent on the amount of free water available within the core concrete; since a greater amount of free water will consume more energy as it vaporises.

Figure 20 shows temperatures observed in the steel tube and at the concrete centreline for two tests in which the core concrete was cured for only 14 and 28 days, respectively (C-1-1-F-I-C1.14D and C-1-1-F-I-C1.28D). The 14-day curing shows slightly lower temperatures after 120 minutes at the steel tube and concrete centreline (70ºC and 120ºC lower, respectively). The 28-day curing temperatures are greater than those seen in the tests performed after 13 months as seen in Table 4, however comparisons are difficult to make due to the different furnaces in which the specimens were tested (as previously discussed). It is generally assumed in the concrete industry that after 28-days the majority (>80%) of the free water has been fixed by the cement paste, and thus without additional research 28 days should be the minimum curing time required for fire testing of CFS sections.

Figure 20 also shows the specific tests used to assess the performance of different DFTs of protection applied to the columns based on required protection times of 75 (C-1-1-F-I-C1.75) and 120 minutes (C-1-1-F-I-C1.120), respectively, again with an assumed limiting steel temperature of 520ºC. These tests are useful in assessing the consistency of the protection material at different thicknesses and understanding the thermal response of the steel and concrete for different thermal response of the coating. The temperatures experienced by the steel after the required protection time in test C-1-1-F-I-C1.75 and C-1-1-F-I-C1.120 were 388 and 387ºC respectively, compared to the 28 day test (due to the similar furnace being used) with 90 minute fire protection in which the

temperatures were 319ºC at 90 minutes. This is thought to be due partly to the very different cure times for the concrete and to the different specimen layouts during testing within the different furnaces.

4.3 Design of Protected CFS Sections

The protected tests presented herein have shown that the specific intumescent coatings used were extremely efficient at protecting CFS columns, with the majority of tests not reaching the limiting temperature of 520ºC more than 30 minutes after the design fire resistance time. Some of the tests experienced cracking and splitting of the protective char layer, but with only localised effects on increasing temperatures within the rest of the cross-sections.

The much lower than expected temperatures for the protected sections clearly indicate that either there are large conservatisms within the prescription and design of the required thickness of fire protection for these specific coatings, or alternatively that the filling of the steel tube with concrete fundamentally changes the thermal response of the coatings. A detailed analysis of the performance of the intumescent on both filled and unfilled sections, as well as a forensic analysis on currently available DFT design methods for determining the effective section factors for CFT columns using data from furnace tests on unfilled steel tubes has been presented elsewhere by the authors [19]. This has demonstrated that the observed conservatism in the current approach to specify design DFTs is due to the inappropriate application of unprotected CFS effective section factors for the prescription of intumescent coatings on protected CFS sections. Until a more rational general method for determining the effective section factors for protected CFS sections is developed, either the current guidance [17] should be used as it is conservative, or appropriate testing conducted to demonstrate the performance of specific intumescent products on CFS sections.

5 Conclusions

This paper has presented furnace tests on 14 unprotected and 20 protected CFS sections, along with thermal modelling of the unprotected sections. The unprotected tests demonstrated that the size and

shape of the section affect the temperatures observed, with larger sections experiencing lower steel and concrete temperatures due to their larger thermal mass. Square sections experienced higher temperatures at their corners, as expected. The temperature differential across the steel-concrete interface was also affected by the section size, with greater temperature differentials recorded in the larger sections since these sections have larger thermal mass thus reducing the concrete temperatures near the interface and promoting earlier formation of an air gap (with associated thermal resistance). The inclusion of steel and polypropylene fibres within the concrete mix had no effect on the heat transfer within the sections

The ability to predict the temperatures within the unprotected CFS sections using available Eurocode guidance [4] is relatively poor, since this approach appears not properly account for; (a) the heat transfer to the steel from the furnace environment; (b) the thermal effect of the air gap at the steel-concrete interface; (c) the variation in effective specific heat, including water vaporisation at different pressures and thus temperatures; and (d) the thermal conductivity of the concrete, for which no guidance is given as to which of the permissible thermal conductivity curves (higher or lower bound) should be adopted.

New modelling approaches for each of the above factors have been presented and shown to more accurately predict the temperatures within CFS sections, with errors generally within ±50^{o}C. This new approach employed; (a) a new equivalent area method for the effective specific heat capacity of concrete to include the effect of water vaporisation; (b) a gap conductance relationship to account for the formation of an air gap; and (c) a temperature dependent emissivity of steel, in conjunction with a reduced fire emissivity of 0.38.

Whilst the predicted temperatures using the new modelling approach showed good agreement with the observed test data, there are key areas of concern for appropriate modelling of heat transfer to CFS sections, especially with respect to the ‘correct’ furnace emissivity value to assume in modelling. To calibrate the predicted temperatures to those observed in the thermal tests, an emissivity of the furnace of 0.38 was required in the current study; this may be appropriate only

for the specific furnace in which the specimens were tested. Other researchers [32] have quoted furnace emissivities of 0.75. Additional research is needed in this area.

The tests on CFS sections protected with intumescent coatings showed similar trends as the unprotected tests, with larger sections experiencing lower temperatures in both the steel and the concrete. The design DFTs calculated using the current UK guidance were seen to be highly conservative in most cases, with peak steel temperatures consistently lower than expected and well below the assumed limiting temperature of 520°C at the design fire resistance time (and remaining below 520°C for at least 30 minutes beyond the required fire resistance time). An assessment of this showed that this is due to the inappropriate assumption that the section factor for unprotected CFS sections will be the same as for protected CFS sections as would be the case for plain steel sections [19].

Of the 24 protected tests performed, only a few experienced any cracking or splitting of the intumescent protective char; in these cases there was a mild, local detrimental effect on the protective ability of the coating, however the overall steel tube temperatures remained below the limiting temperature. The age of the concrete at the time of testing had a mild influence on the thermal responses observed, with 14-day old CFS sections showing lower (160°C at concrete centreline TC) temperatures than those in which the concrete was at least 28-days old. It is recommended that 28 days be the minimum age of a CFS section prior to fire testing.

If the conservatisms which are inherent in the current approach for the specification of design DFTs for intumescent protection of CFS sections are to be avoided additional analytical work and experimental testing of these types of sections is needed.

6 Acknowledgments

The authors gratefully acknowledge the support of International Paint Ltd, Ove Arup & Partners (Technology Practices), The Ove Arup Foundation, The Royal Academy of Engineering, the UK Engineering and Physical Sciences Research Council, and the School of Engineering at the University of Edinburgh.

References

[1] V. Kodur, "Guidelines for fire resistant design of concrete filled steel HSS columns: State-of-the-art and research needs," *Int. J. Steel Struct.*, vol. 7, no. 3, pp. 173–182, 2007.

[2] Communities and Local Government, "Approved Document B – Volume 2 – Buildings other than dwelling houses," London, UK, 2007.

[3] T. Lennon, D. B. Moore, Y. C. Wang, and C. G. Bailey, *Designers' guides to the Eurocodes*. London, UK: Thomas Telford Publishing, 2007.

[4] CEN, "BS EN 1994-1-2: Eurocode 4: Design of composite steel and concrete structures; Part 1-2: Structural Fire Design," Brussels, Belgium, 2005.

[5] Y. C. Wang and A. Orton, "Fire resistant design of concrete filled tubular steel columns," *Struct. Eng.*, vol. 7, no. October, pp. 40–45, 2008.

[6] J. M. Aribert, C. Renaud, and B. Zhao, "Simplified fire design for composite hollow-section columns," in *Proceedings Of The Institution Of Civil Engineers - Structures and Buildings*, 2008, vol. 161,6, no. December, pp. 325–336.

[7] D. I. Rush, L. A. Bisby, and A. Jowsey, "Post-fire residual capacity of protected and unprotected concrete filled steel hollows columns," in *8th International Conference on Structures in Fire*, 2014, pp. 435 – 442.

[8] D. Rush, L. Bisby, A. Jowsey, A. Melandinos, and B. Lane, "Structural performance of unprotected concrete-filled steel hollow sections in fire: A review and meta-analysis of available test data," *Steel Compos. Struct.*, vol. 12, no. 4, pp. 325–350, Apr. 2012.

[9] L. H. Han, Y. F. Yang, and L. Xu, "An experimental study and calculation on the fire resistance of concrete-filled SHS and RHS columns," *J. Constr. Steel Res.*, vol. 59, no. 4, pp. 427–452, Apr. 2003.

[10] V. K. R. Kodur and T. T. Lie, "Fire Performance of Concrete-Filled Hollow Steel Columns," *J. Fire Prot. Eng.*, vol. 7, no. 3, pp. 89–97, Jan. 1995.

[11] Z. Tao and M. Ghannam, "Heat transfer in concrete-filled carbon and stainless steel tubes exposed to fire," *Fire Saf. J.*, vol. 61, pp. 1–11, Oct. 2013.

[12] L. H. Han, L. Xu, and X. L. Zhao, "Tests and analysis on the temperature field within concrete filled steel tubes with or without protection subjected to a standard fire," *Adv. Struct. Eng.*, vol. 6, no. 2, pp. 121–133, 2003.

[13] D. Madrzykowski and D. W. Stroup, "Flammability Hazard of Materials," in *Fire Protection Handbook*, 20th Edit., vol. 11, no. 2, NFPA, 2008, pp. 2/31–48.

[14] CEN, "BS EN 13381-6:2012 - Test methods for determining the contribution to the fire resistance of structural members: Part 6: Applied protection to concrete filled hollow steel columns," Brussels, Belgium, 2012.

[15] ISO, "ISO 834: Fire resistance tests-elements of building construction," Geneva, Switzerland, 1999.

[16] CEN, “BS EN 1991-1-2:2002 Eurocode 1- Actions on structures; Part 1-2: General Actions - Actions on structures exposed to fire,” Brussels, Belgium, 2009.

[17] S. J. Hicks, G. M. Newman, M. Edwards, and A. Orton, “Design guide for SHS concrete filled columns,” Corus Tubes, Corby, Northants, 2002.

[18] CEN, “BS EN 1993-1-2:2005: Eurocode 3: Design of steel stuctures; Part 1-2: General rules - Structural fire design,” Brussels, Belgium, 2009.

[19] D. Rush, L. Bisby, M. Gillie, A. Jowsey, and B. Lane, “Design of intumescent fire protection for concrete filled structural hollow sections,” *Fire Saf. J.*, vol. 67, pp. 13–23, Jul. 2014.

[20] CEN, “BS EN 13381-8:2010: Test methods for determining the contribution to the fire reistance of structural members; Part 8: Applied reactive protection to steel members,” Brussels, Belgium, 2010.

[21] British Standards Institution, “BS 476-20: 1987 - Fire tests on building materials and structures — Part 20: Method for determination of the fire resistance of elements of construction (general principals),” 2014.

[22] D. Rush, “Fire performance of unprotected and protected concrete filled structural hollow sections,” University of Edinburgh, 2013.

[23] J. Ghojel, “Experimental and analytical technique for estimating interface thermal conductance in composite structural elements under simulated fire conditions,” *Exp. Therm. Fluid Sci.*, vol. 28, no. 4, pp. 347–354, Mar. 2004.

[24] D. Rush, L. Bisby, and E. O’Loughlin, “Concrete-filled structural hollow sections in fire: accounting for heat transfer across a gap,” in *15th International conference on Experimental Mechanics*, 2012, p. 17pp.

[25] T. Paloposki and L. Liedquist, *Steel emissivity at high temperatures - Research notes*. Tampere, Finland: Technical Research Centre of Finland, 2005.

[26] J. L. Torero, “Assesing the true performance of structures in fire.,” in *First international conference of performance-based and life-cycle structural engineering, 5-7 December*, 2012, pp. 429–440.

[27] British Standards Institution, “BS 5950-8:2003 Structural use of steelwork in buildings - Part 8; Code of Practice for fire resistant design,” 2003.

[28] Association for Specialist Fire Protection, *YELLOW BOOK: Fire protection for structural steel in buildings*, 5th Edit., vol. 1. Association for Specialist Fire Protection, 2014.

[29] J. E. J. Staggs, “Thermal conductivity estimates of intumescent chars by direct numerical simulation,” *Fire Saf. J.*, vol. 45, no. 4, pp. 228–237, 2010.

[30] The Concrete Society, *Assessment, design and repair of fire-damaged concrete structures - Technical report no. 68*. Camberley UK: The Concrete Society, 2008.

[31] C. Maluk, L. Bisby, G. Terrasi, M. Krajcovic, and J. Torero, “Novel fire testing methodology: Why, how and what now?,” *First Int. Conf. performance-based life-cycle Struct. Eng. 5-7 December*, pp. 448–458, 2012.

[32] T. T. Lie, M. Chabot, and R. J. Irwin, *Fire resistance of circular hollow steel sections filled with bar-reinforced concrete - Internal Report No. 636*. Ottawa, Canada: National Research Council Canada, 1992.

Table 1: Testing matrix

Test no.[a]		Shape[b]	Size (b OR d) (mm)	t_a (mm)	Fill[c]	Fire[d]	Reactive coating					
							Section Factor				DFT (mm)[g]	
							Type[e]	F.R.[f] (min)	$t_{a,e}$ (mm)	H_p/A_{eff} (m^{-1})	Design	Applied
1	C-3-3-F-I-N	C	323.9	10	F	I	N	N/A				
2	C-3-2-F-I-N	C	323.9	8	F	I	N					
3	C-2-3-F-I-N	C	219.1	5	F	I	N					
4	C-2-2-F-I-N	C	219.1	8	F	I	N					
5	C-2-1-F-I-N	C	219.1	10	F	I	N					
6	C-1-3-F-I-N	C	139.7	10	F	I	N					
7	C-1-2-F-I-N	C	139.7	8	F	I	N					
8	C-1-1-H-I-N	C	139.7	5	H	I	N					
9	C-1-1-F-I-N	C	139.7	5	F	I	N					
10	S-3-3-F-I-N	S	300	10	F	I	N					
11	S-1-3-F-I-N	S	120	10	F	I	N					
12	S-1-1-F-I-N	S	120	5	F	I	N					
13	C-1-1-F-S-N	C	139.7	5	F	S	N					
14	S-1-1-F-S-N	S	120	5	F	S	N					
15	C-3-3-F-I-C1a	C	323.9	10	F	I	C1	90	27.1	36.9	3.39	3.50
16	C-3-3-F-I-C1b	C	323.9	10	F	I	C1	90	27.1	36.9	3.39	3.60
17	C-3-2-F-I-C1	C	323.9	8	F	I	C1	90	25.1	39.9	3.43	3.48
18	C-2-3-F-I-C1	C	219.1	5	F	I	C1	90	22.1	45.3	3.48	3.50
19	C-2-2-F-I-C1	C	219.1	8	F	I	C1	90	25.1	39.9	3.43	3.50
20	C-2-1-F-I-C1	C	219.1	10	F	I	C1	90	27.1	36.9	3.43	3.55
21	C-1-3-F-I-C1	C	139.7	10	F	I	C1	90	27.1	36.9	3.48	3.53
22	C-1-2-F-I-C1	C	139.7	8	F	I	C1	90	25.1	39.9	3.48	3.52
23	C-1-1-F-I-C1	C	139.7	5	F	I	C1	90	22.1	45.3	3.48	3.51
24	C-1-1-H-I-C1	C	139.7	5	H	I	C1	90	22.1	45.3	3.48	3.53
25	S-3-3-F-I-C1	S	300	10	F	I	C1	90	27.1	36.9	3.39	3.53
26	S-1-1-F-I-C1	S	120	5	F	I	C1	90	21.5	46.5	3.48	3.49
27	C-1-1-F-I-C1.14D	C	139.7	5	F	I	C1	90	22.1	45.3	3.48	3.53
28	C-1-1-F-I-C1.28D	C	139.7	5	F	I	C1	90	22.1	45.3	3.48	3.53
29	C-1-1-F-I-C1.75	C	139.7	5	F	I	C1	75	20.6	48.6	2.10	2.00
30	C-1-1-F-I-C1.120	C	139.7	5	F	I	C1	120	24.5	40.9	4.00	4.06
31	C-1-1-F-S-C1	C	139.7	5	F	S	C1	90	22.1	45.3	3.48	3.53
32	S-1-1-F-S-C1	S	120	5	F	S	C1	90	21.5	46.5	3.48	3.41
33	C-3-3-F-I-C2	C	323.9	10	F	I	C2	90	27.1	36.9	2.94	2.94
34	S-3-3-F-I-C2	S	300	10	F	I	C2	90	27.1	36.9	2.94	3.11

[a] test numbering system *Shape – size – wall thickness- fill type – fire insult –protection type;*
[b] *C* = circle, *S* = square;
[c] *H* = high strength concrete (HSC), *F* = fibre reinforced concrete (FIB);
[d] I = *ISO 834* standard fire insult [15], S = smouldering curve [16];
[e] *N* = unprotected, *C1* = Interchar1120, *C2* = Interchar212;
[f] *F.R.* = required fire resistance based on steel limiting temperature of 520°C; and
[g] DFT = dry film thickness.

Table 2: Predicted temperatures in *unprotected* sections after 30, 90 and 120 minutes of heating for the steel tube, concrete face, and concrete centre TC locations

Test		*Eurocode modelling approach*									*Improved modelling approach*								
		Steel (˚C)			Concrete face (˚C)			Centre (˚C)			Steel (˚C)			Concrete face (˚C)			Centre (˚C)		
		30	90	120	30	90	120	30	90	120	30	90	120	30	90	120	30	90	120
Circular sections exposed ISO 834 standard fire [15]																			
1	C-3-3-F-I-N	666	967	1020	603	828	985	22	75	101	400	870	958	226	709	829	24	101	133
2	C-3-2-F-I-N	684	968	1021	621	834	986	21	73	100	431	885	962	245	727	836	24	101	133
3	C-2-3-F-I-N	677	974	1027	617	842	999	43	127	362	405	887	980	234	747	874	49	181	364
4	C-2-2-F-I-N	693	975	1027	633	846	1000	42	123	344	434	898	984	253	761	879	49	181	361
5	C-2-1-F-I-N	715	976	1028	656	852	1000	40	118	318	498	910	988	296	779	886	50	181	357
6	C-1-3-F-I-N	697	988	1038	643	872	1026	104	673	828	433	932	1012	268	839	956	121	557	734
7	C-1-2-F-I-N	707	987	1038	656	873	1025	104	652	809	464	938	1013	290	847	957	121	554	726
8	C-1-1-F-I-N	726	988	1038	674	876	1025	102	622	781	528	945	1014	335	856	958	122	549	715
9	C-1-1-H-I-N	726	988	1038	674	876	1025	102	622	781	528	945	1014	335	856	958	122	549	715
Square sections exposed to ISO 834 standard fire [15]																			
10	S-3-3-F-I-N	650	958	1013	567	793	958	21	74	100	393	850	951	206	649	776	24	100	132
		(709)	(988)	(1037)	(689)	(899)	(1032)				(435)	(909)	(996)	(327)	(856)	(959)			
11	S-1-3-F-I-N	697	989	1039	619	861	1023	110	743	884	454	939	1018	253	834	951	128	621	791
		(721)	(995)	(1042)	(703)	(910)	(1040)				(471)	(949)	(1024)	(356)	(910)	(1001)			
12	S-1-1-F-I-N	721	988	1038	644	860	1020	106	686	836	554	947	1019	317	843	950	128	605	765
		(748)	(996)	(1043)	733	(917)	1041				(580)	(960)	(1028)	(454)	(926)	(1006)			
Square and Circular sections exposed to smouldering curve [16]																			
13	C-1-1-F-S-N	395	942	1007	348	773	990	75	498	696	305	877	976	168	760	904	76	428	627
14	S-1-1-F-S-N	394	941	1007	330	751	984	84	566	756	295	885	981	155	746	894	82	478	678
		(427)	(954)	(1014)	(406)	(830)	(1011)				(304)	(903)	(992)	(202)	(852)	(964)			

Bracketed number, i.e. (NUM), represent diagonal temperature measurements within square sections

Table 3: Selected observed temperatures in *unprotected* sections after 30, 90, and 120 minutes, as well as maximum temperatures, for the steel tube, concrete face, 35 mm depth and concrete centre TC locations

Test		Steel (˚C)					Concrete face (˚C)					35 mm depth (˚C)					Centre (˚C)				
		30	90	120	Max	Time	30	90	120	Max	Time	30	90	120	Max	Time	30	90	120	Max	Time
Circular sections exposed ISO 834 standard fire [15]																					
1	C-3-3-F-I-N	489	875	949	949	120	241	721	828	828	120	109	412	541	559	127	22	121	132	313	239
2	C-3-2-F-I-N	479	862	931	931	120	250	721	828	828	120	101	380	504	525	128	22	119	134	294	240
3	C-2-3-F-I-N	513	902	981	981	120	272	751	869	869	120	120	452	616	648	131	48	193	377	570	175
4	C-2-2-F-I-N	503	887	971	971	120	285	770	885	885	120	131	487	637	659	127	47	180	330	537	182
5	C-2-1-F-I-N	531	889	973	973	120	323	777	892	892	120	141	482	628	649	127	50	178	331	529	180
6	C-1-3-F-I-N	554	944	1005	1005	119	444	924	995	995	119	283	807	924	924	120	145	684	844	871	131
7	C-1-2-F-I-N	529	925	991	992	119	394	896	977	977	120	179	792	913	913	120	116	737	882	888	124
8	C-1-1-F-I-N	532	926	997	997	120	371	860	954	954	120	136	647	808	834	131	123	564	756	820	140
9	C-1-1-H-I-N	553	927	996	996	120	380	859	952	952	120	157	651	808	835	131	138	574	754	822	142
Square sections exposed to ISO 834 standard fire [15]																					
10	S-3-3-F-I-N	506	886	966	966	120	218	671	782	782	120	95	346	462	480	129	21	116	139	309	240
		(506)	(893)	(975)	(975)	(120)	(291)	(823)	(928)	(928)	(120)	(139)	(556)	(699)	(713)	(125)					
11	S-1-3-F-I-N	458	913	987	987	120	320	870	961	961	120	155	719	875	890	126	145	698	865	886	127
		(479)	(922)	(995)	(995)	(120)	(356)	(891)	(977)	(977)	(120)	(169)	(741)	(886)	(897)	(126)					
12	S-1-1-F-I-N	465	895	974	974	120	317	829	932	932	120	147	653	821	847	129	139	556	699	713	125
		(513)	(912)	(984)	(985)	(119)	(305)	(822)	(928)	(928)	(120)	(161)	(696)	(850)	(864)	(125)					
Square and Circular sections exposed to smouldering curve [16]																					
13	C-1-1-F-S-N	320	893	980	980	120	187	820	935	935	120	86	543	749	787	133	66	448	683	773	145
14	S-1-1-F-S-N	296	905	990	990	120	175	808	935	935	120	90	569	793	830	129	78	529	766	826	134
		(260)	(897)	(987)	(987)	(120)	(206)	(877)	(978)	(978)	(120)	(94)	5(92)	(807)	(837)	(128)					

Bracketed number, i.e. (NUM), represent diagonal temperature measurements within square sections

Table 4: Selected observed temperatures of *protected* CFS sections after 30, 90, and 120 minutes, as well as maximum temperatures, for the steel tube, concrete face, 35 mm depth and concrete centre TC locations

	Test	Steel (°C)					Concrete face (°C)					35 mm depth (°C)					Centre (°C)				
		30	90	120	Max	Time	30	90	120	Max	Time	30	90	120	Max	Time	30	90	120	Max	Time
Protected circular sections exposed ISO 834 standard fire [15]																					
15	C-3-3-F-I-C1a	122	204	244	244	120	94	166	200	200	128	58	124	153	160	146	22	60	86	145	238
16	C-3-3-F-I-C1b	125	206	246	246	120	92	163	196	199	127	57	120	149	158	143	21	57	80	143	239
17	C-3-2-F-I-C1	131	202	238	239	122	91	159	188	192	128	57	120	148	156	138	21	54	76	139	236
18	C-2-3-F-I-C1	124	210	254	255	122	91	169	204	209	131	66	141	167	181	177	36	107	142	166	216
19	C-2-2-F-I-C1	126	204	275	285	128	99	176	235	251	135	69	145	207	245	150	39	114	136	203	239
20	C-2-1-F-I-C1	132	230	283	283	120	102	188	233	234	124	67	145	175	181	165	37	109	147	170	167
21	C-1-2-F-I-C1	133	247	320	375	183	116	206	272	358	189	88	147	212	350	217	79	140	170	349	226
22	C-1-2-F-I-C1	132	259	350	389	182	118	242	332	387	183	101	193	277	373	187	106	180	254	361	195
23	C-1-1-F-I-C1	140	264	366	403	181	123	237	333	397	183	90	178	259	380	191	74	137	169	340	228
24	C-1-1-H-I-C1	125	234	311	348	182	111	203	272	337	183	77	154	186	319	204	67	141	166	317	216
Protected square sections exposed to ISO 834 standard fire [15]																					
25	S-3-3-F-I-C1	118	193	230	230	123	79	140	173	176	132	44	99	130	150	218	21	57	82	140	238
		(133)	(228)	(275)	(275)	(120)	(101)	(180)	(219)	(220)	(125)	(71)	(143)	(169)	(172)	(139)					
26	S-1-1-F-I-C1	136	241	316	317	121	112	210	267	283	179	82	171	191	281	211	76	169	180	281	216
		(134)	(243)	(311)	(311)	(122)	(123)	(225)	(288)	(296)	(126)	(89)	(173)	(205)	(281)	(205)					
Protected circular sections exposed ISO 834 standard fire [15] (age and protection thickness tests)																					
27	C-1-1-F-I-C1.14D	141	272	386	404	125	122	241	343	371	133	97	201	277	365	214	89	202	266	365	214
28	C-1-1-F-I-C1.28D	161	319	458	470	126	142	297	432	452	130	112	275	402	435	137	106	261	394	432	138
29	C-1-1-F-I-C1.75	184	461	603	608	121	150	381	531	542	136	106	251	390	509	186	90	179	326	514	198
30	C-1-1-F-I-C1.120	149	270	387	620	183	129	242	343	579	197	80	156	214	576	252	77	151	192	525	252
Protected square and circular sections exposed to smouldering curve [16]																					
31	C-1-1-F-S-N	125	250	352	380	163	110	227	326	375	179	100	204	302	368	182	100	202	300	366	180
32	S-1-1-F-S-N	116	241	390	396	122	103	210	332	349	127	74	171	192	320	179	69	168	186	322	178
		(119)	(283)	(472)	(472)	(120)	(110)	(243)	(414)	(417)	(121)	(80)	(174)	(203)	(317)	(179)					
Protected square and circular sections exposed to ISO 834 standard fire [15]																					
33	C-3-3-F-I-C2	202	317	397	398	121	129	223	300	310	129	75	156	186	224	169	21	70	109	160	240
34	S-3-3-F-I-C2	207	317	398	398	120	126	225	289	299	129	67	151	179	220	190	20	82	109	159	239
		(226)	(387)	(484)	(484)	(120)	(167)	(319)	(408)	(410)	(122)	(93)	(191)	(250)	(280)	(144)					

Bracketed number, i.e. (NUM), represent diagonal temperature measurements within square sections

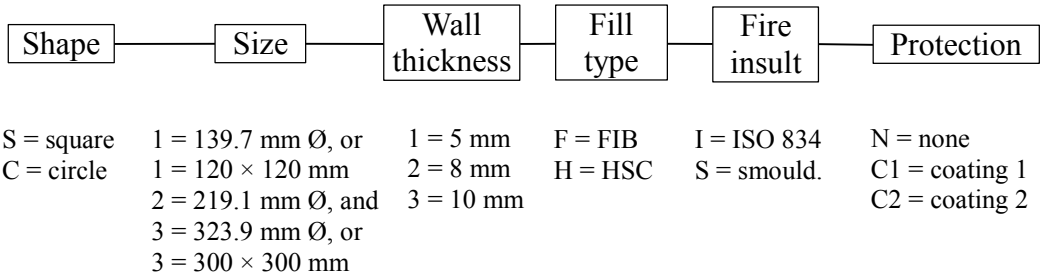

Figure 1: Details of six-character naming and identification scheme for the columns tested

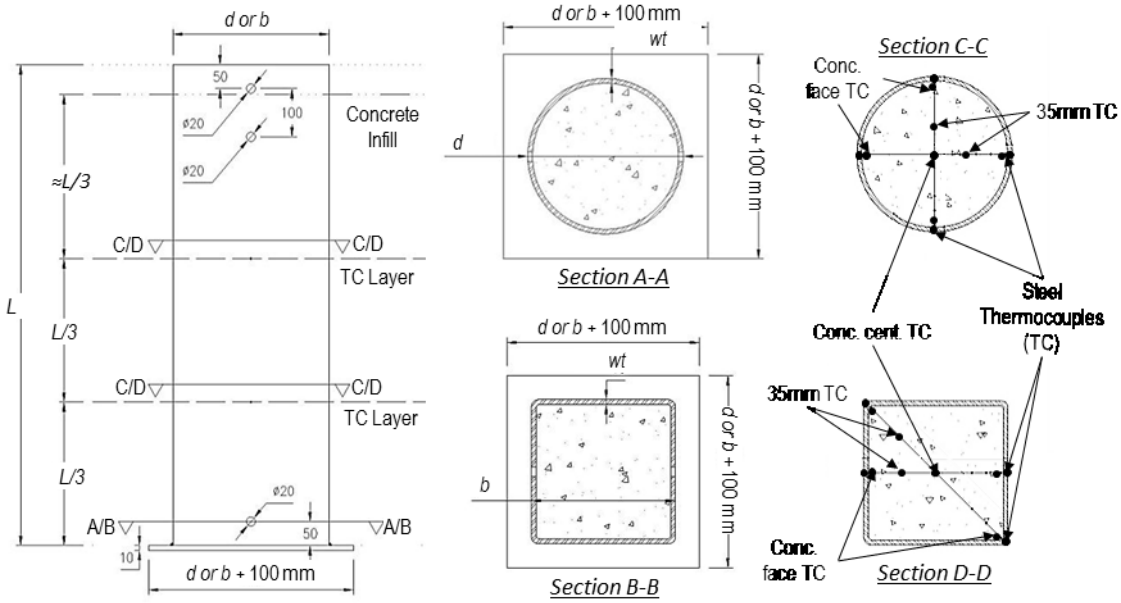

Figure 2: Specimen schematic layout

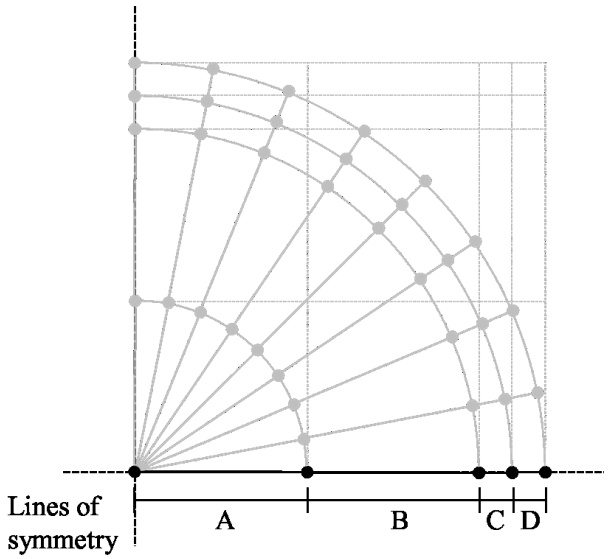

Figure 3: Mesh region diagram for thermal predictions

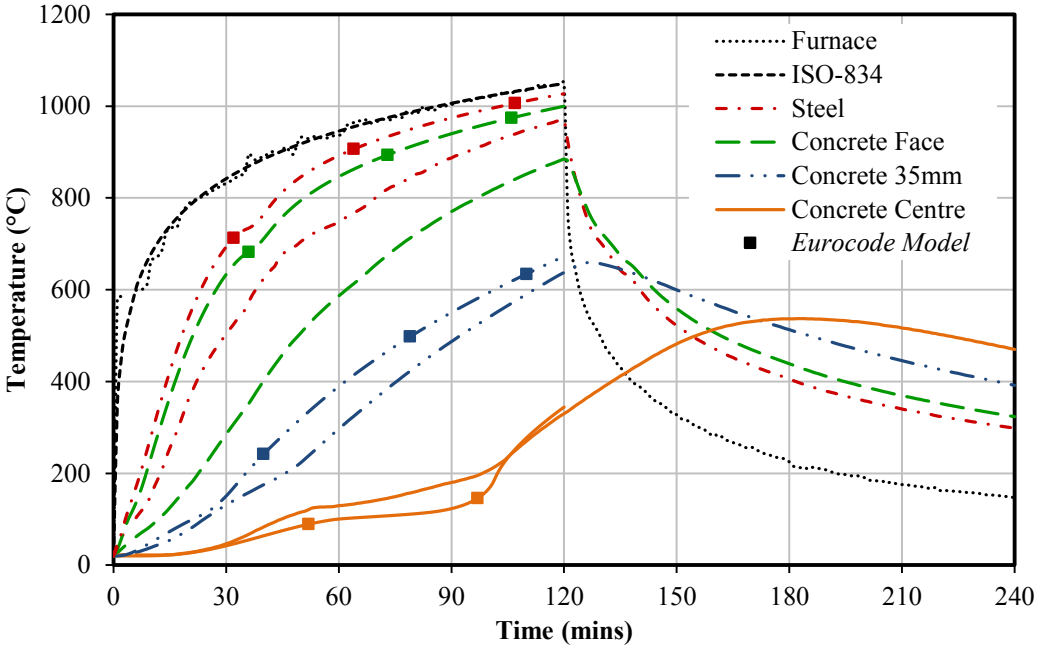

Figure 4: Representative observed and *Eurocode* model predicted temperatures for test C-2-2-F-I-N under exposure to an ISO 834 standard fire

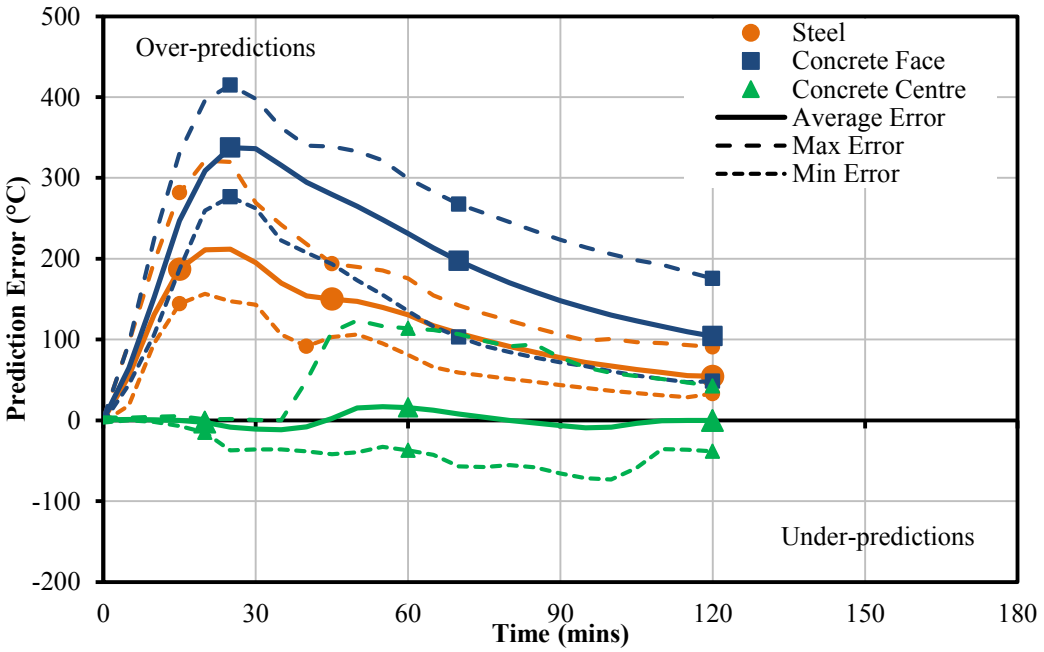

Figure 5: Difference between the *Eurocode* model predictions and observed temperatures for unprotected tests exposed to the ISO-834 fire curve (x-x-x-x-I-N)

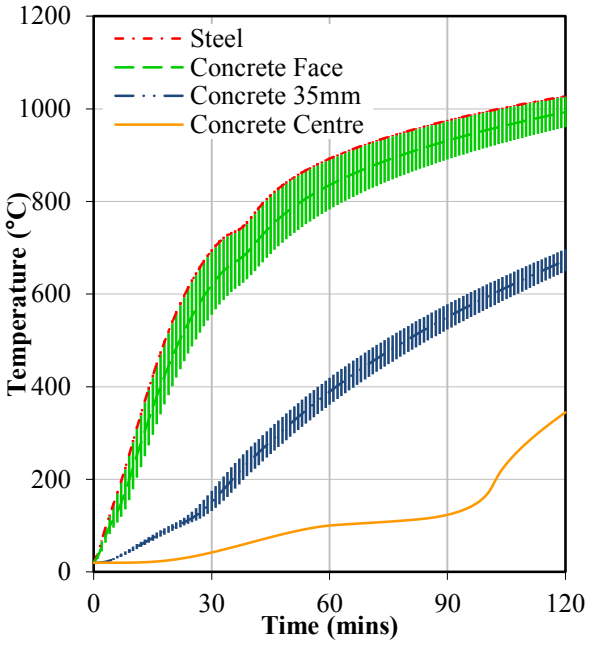

Figure 6: Predicted temperatures with assumed TC placement errors of ±2.5 mm for Test C-2-2-F-I-N using *Eurocode* thermal modelling approach

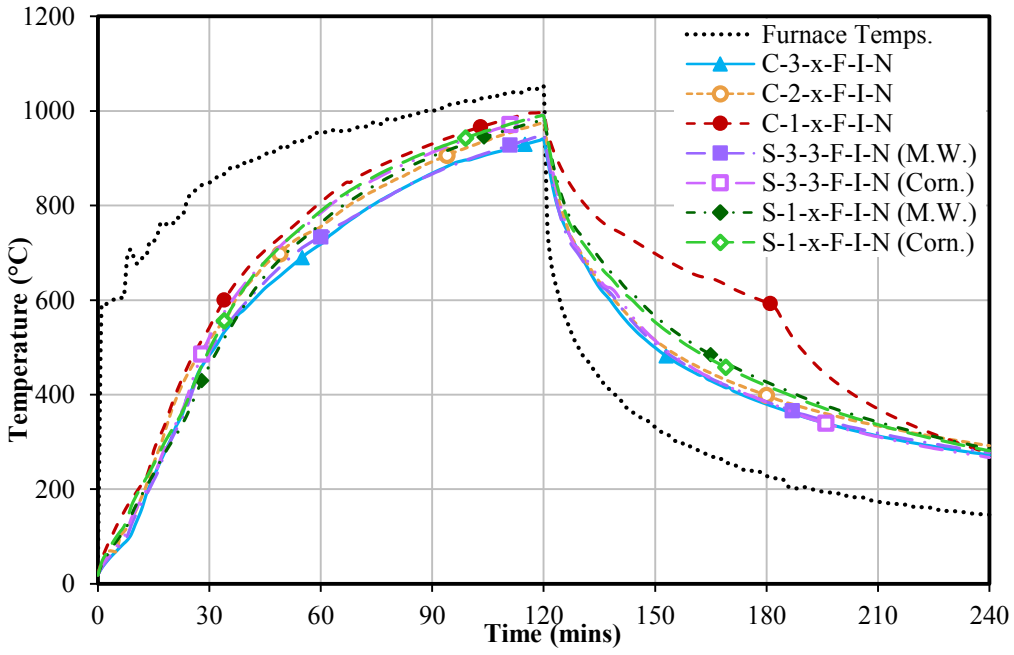

Figure 7: Observed steel tube temperatures of the unprotected sections exposed to the ISO-834 fire curve

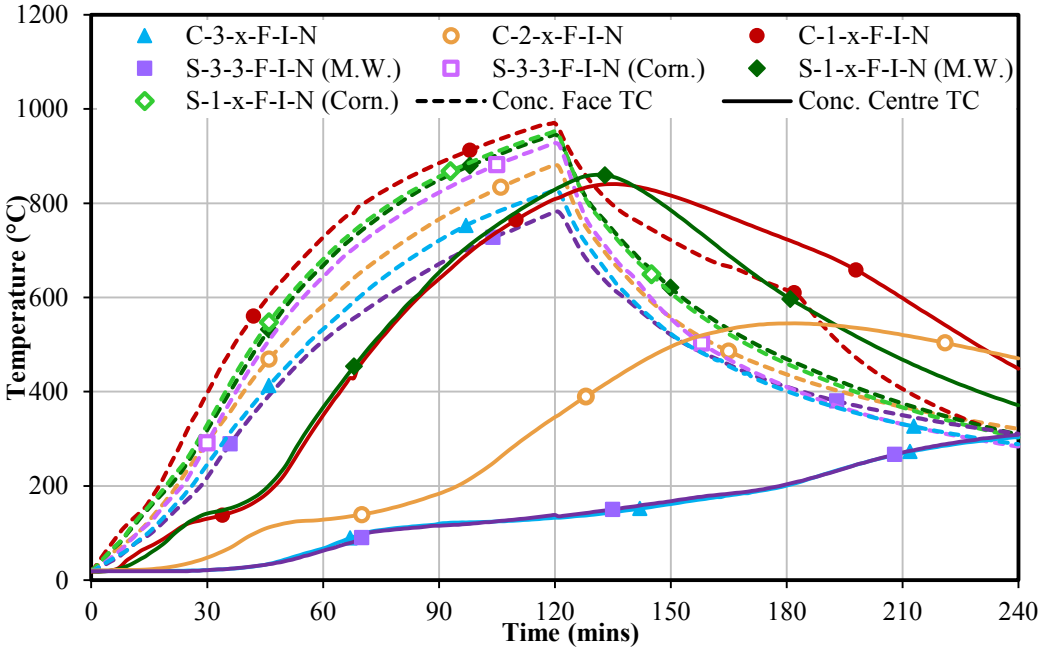

Figure 8: Observed temperatures at the concrete face and concrete centre thermocouples (TCs) for S-x-x-F-I-N and C-x-x-F-I-N sections

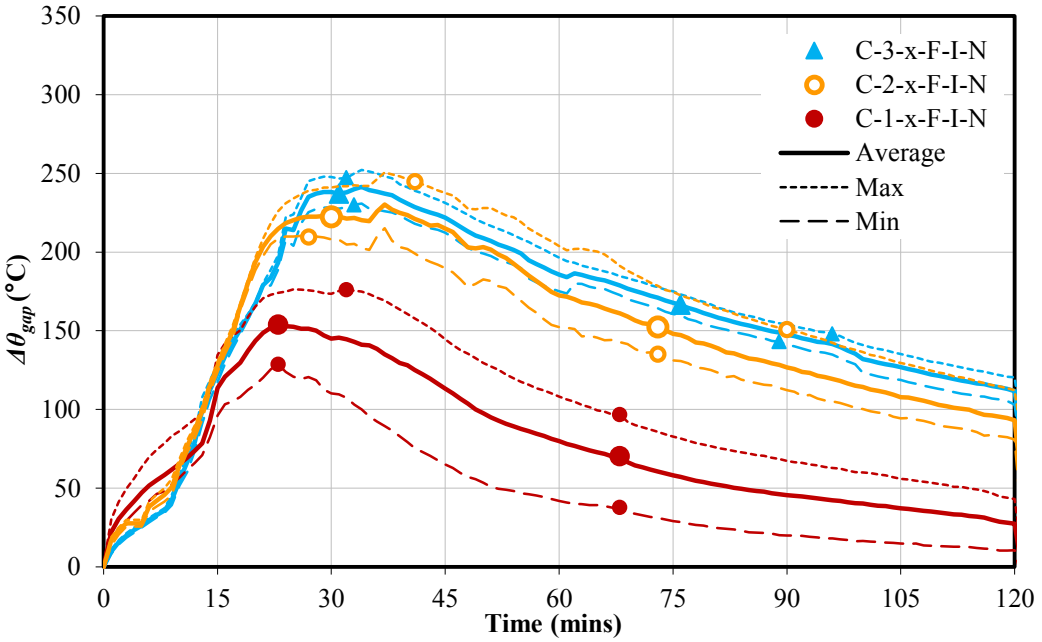

Figure 9: Differential interface temperatures, $\Delta\theta_{gap}$, for unprotected circular CFS sections (C-x-x-F-I-N)

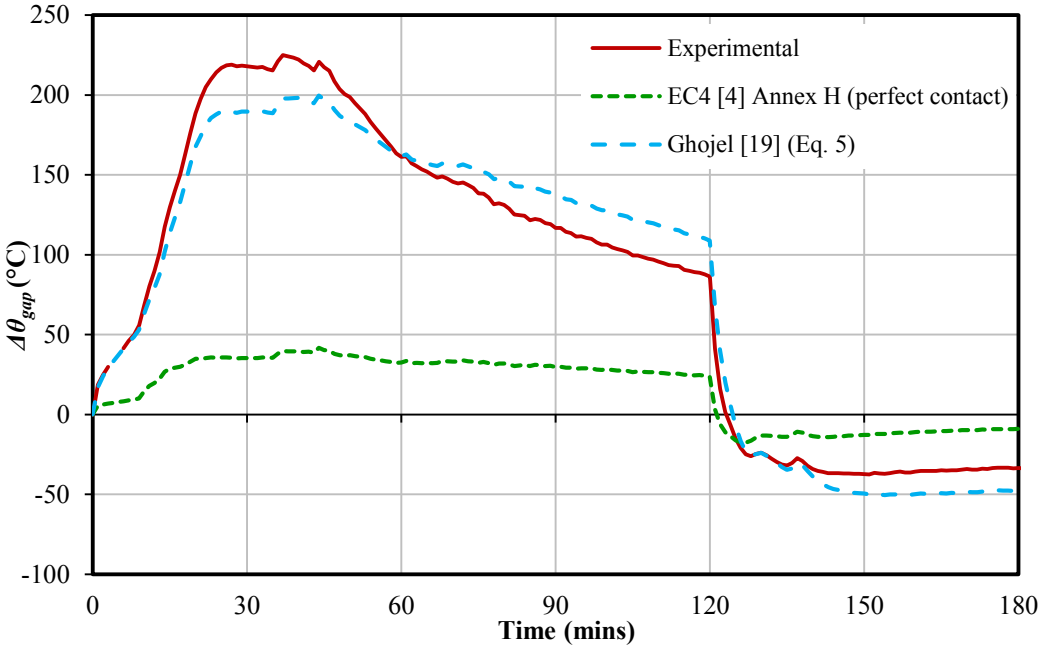

Figure 10: Observed and predicted (using observed steel temperatures) differential gap temperatures for test C-2-2-F-I-N

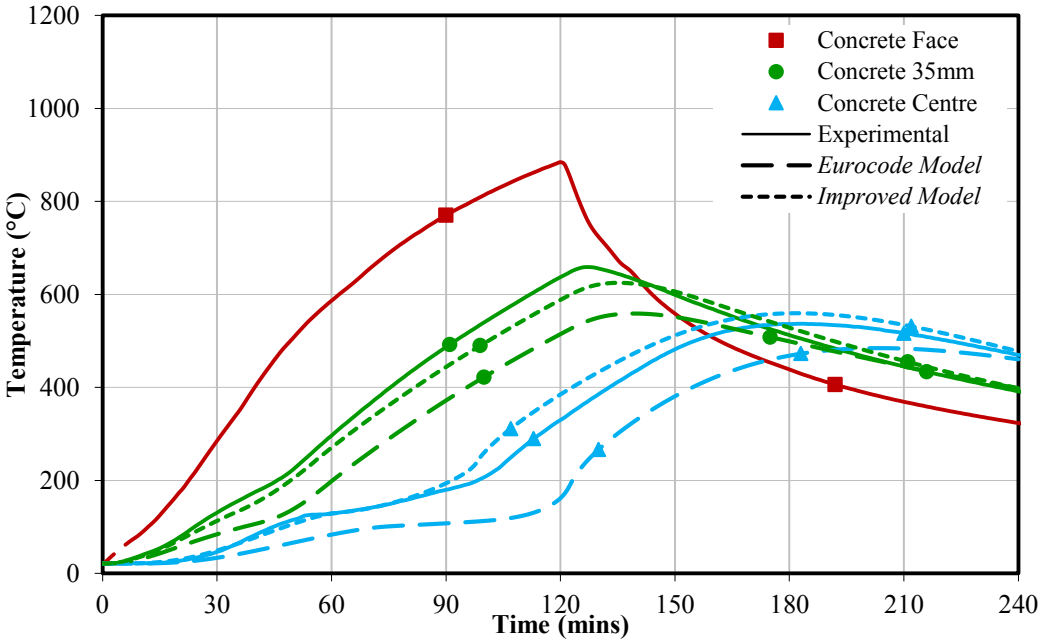

Figure 11: Predicted and observed temperature at various depths in the concrete core for test C-2-2-F-I-N using the *Eurocode* and *Improved* modelling approaches with imposed experimental concrete surface temperatures

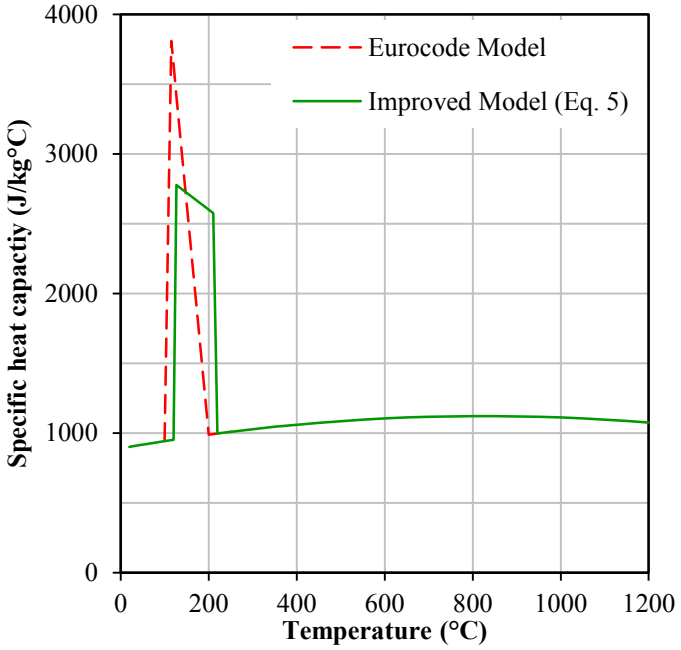

Figure 12: Specific heat capacity models for concrete based on the EC4 [4] **temperature dependent model and the *Improved* modelling approach (Equation 6) with 6.5% moisture content**

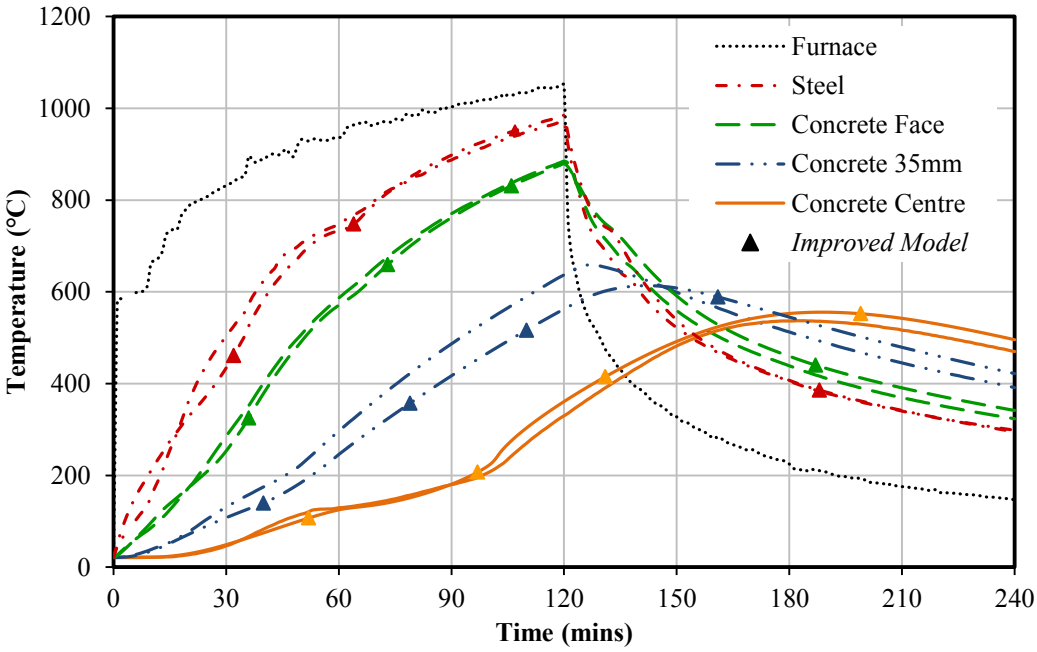

Figure 13: Observed and predicted temperatures for test C-2-2-F-I-N using the *Improved* modelling approach

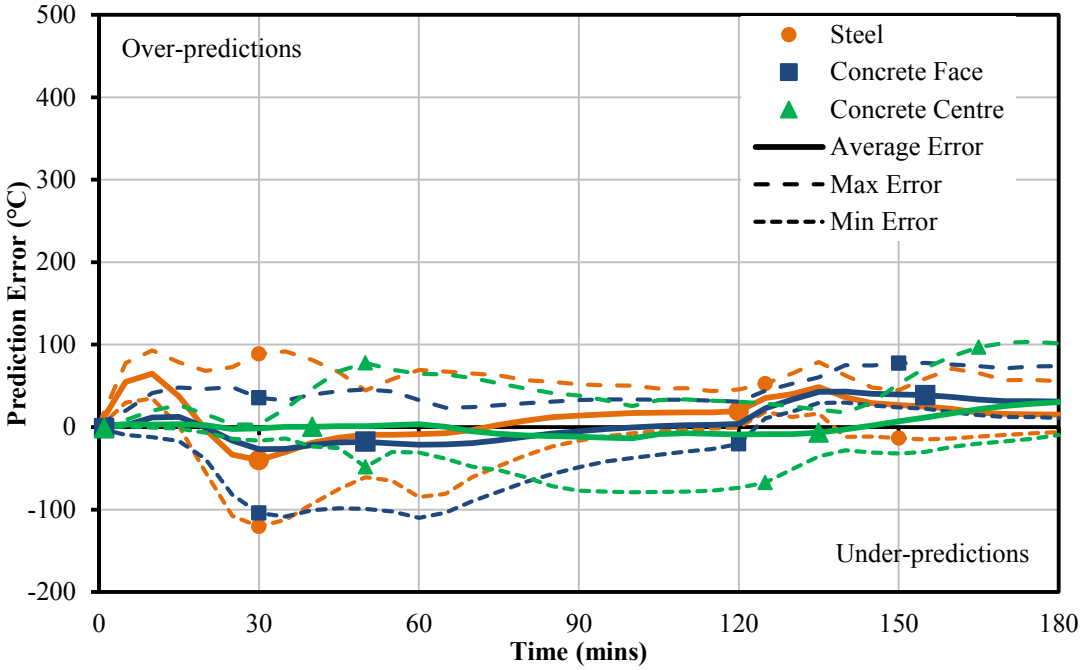

Figure 14: Difference between the *Improved* predictions and observed temperatures for unprotected tests exposed to the ISO-834 fire curve (x-x-x-x-I-N)

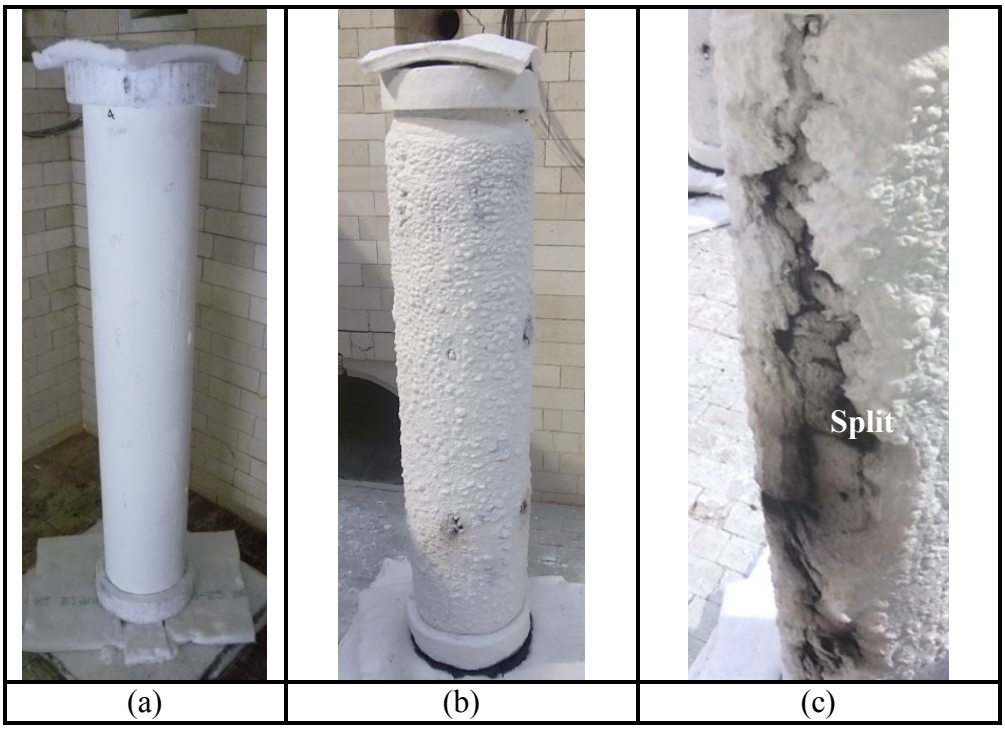

Figure 15: Intumescent coating appearance of (a) C-2-2-F-I-C1 before heating, (b) C-2-1-F-I-C1 after heating and (c) C-2-2-F-I-C1 after heating with split in char

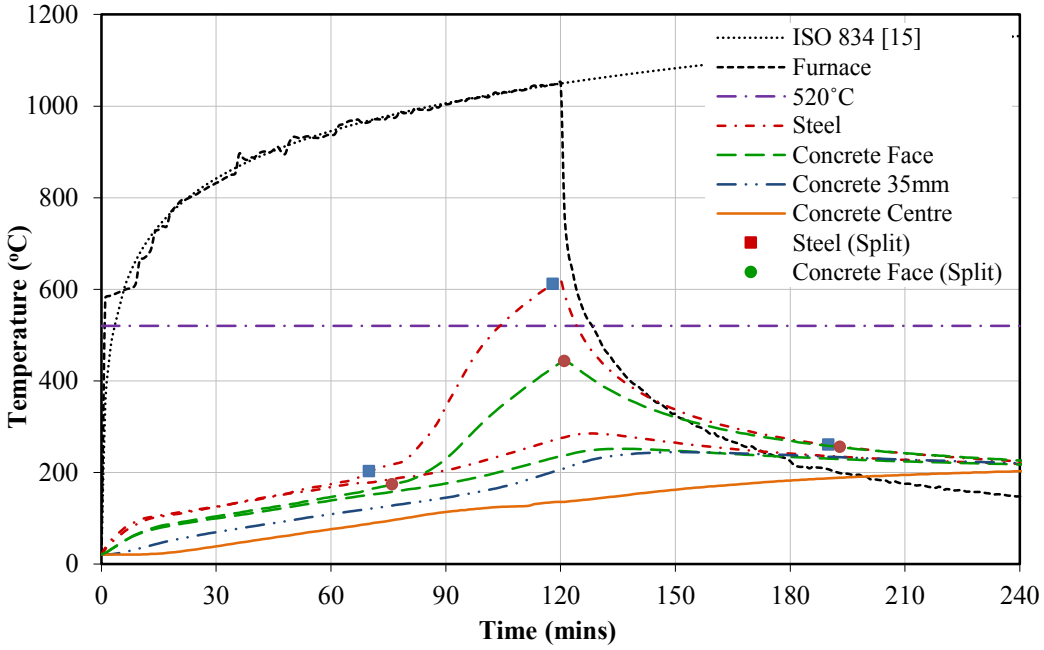

Figure 16: Representative temperatures within a protected CFS section under ISO 834 standard fire exposure (C-2-2-F-I-C1)

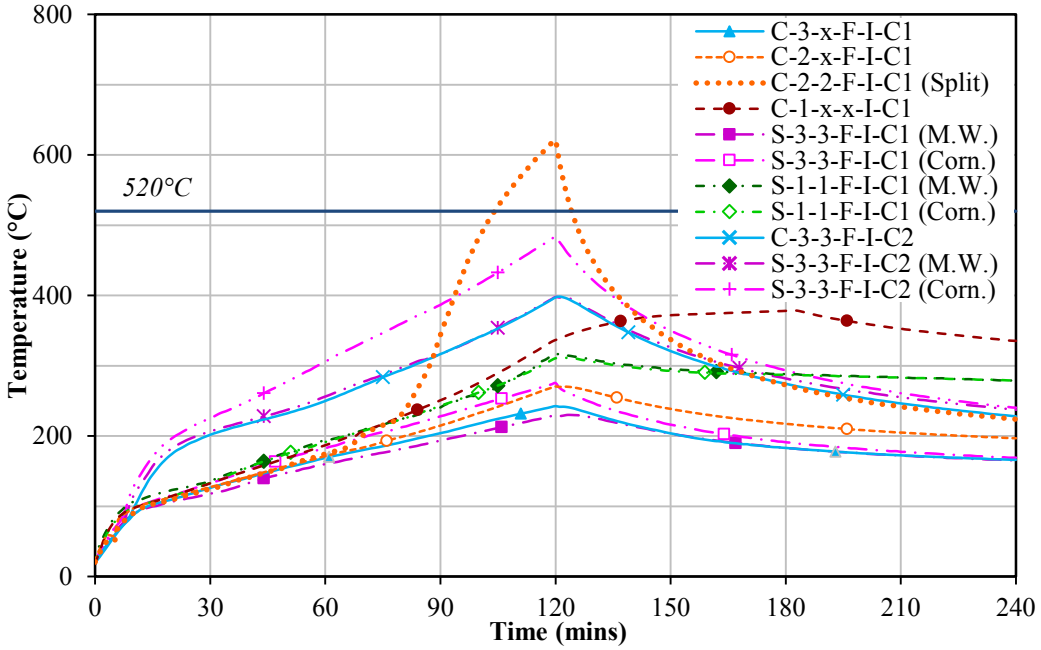

Figure 17: Observed protected test steel temperatures with a design F.R. of 90 minutes to 520ºC for both C1 and C2 coating types

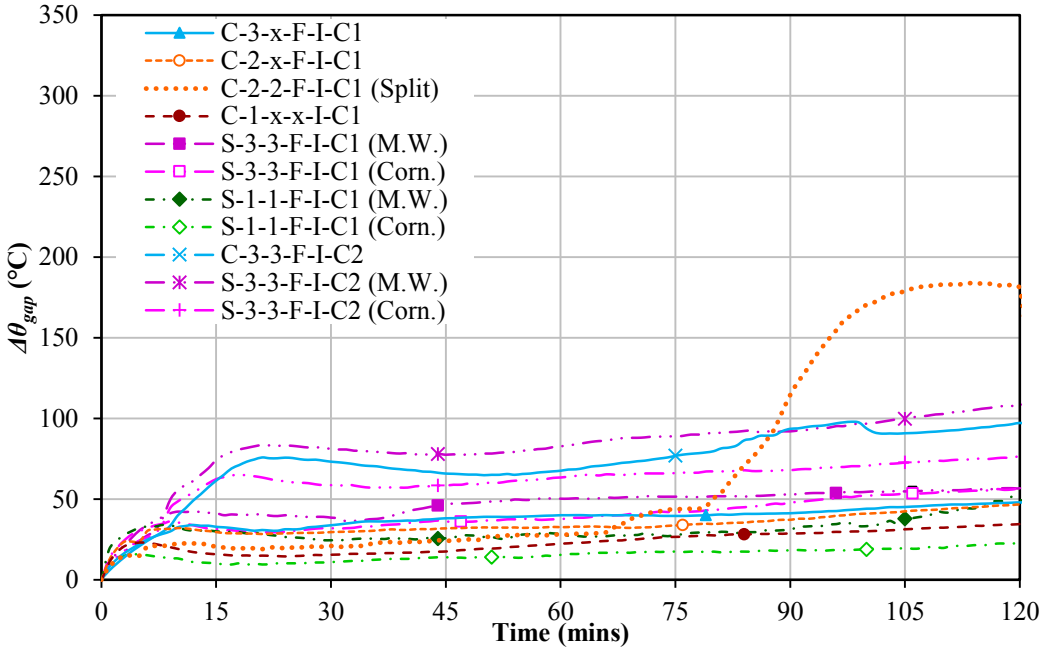

Figure 18: Observed differential gap temperatures for the protected tests

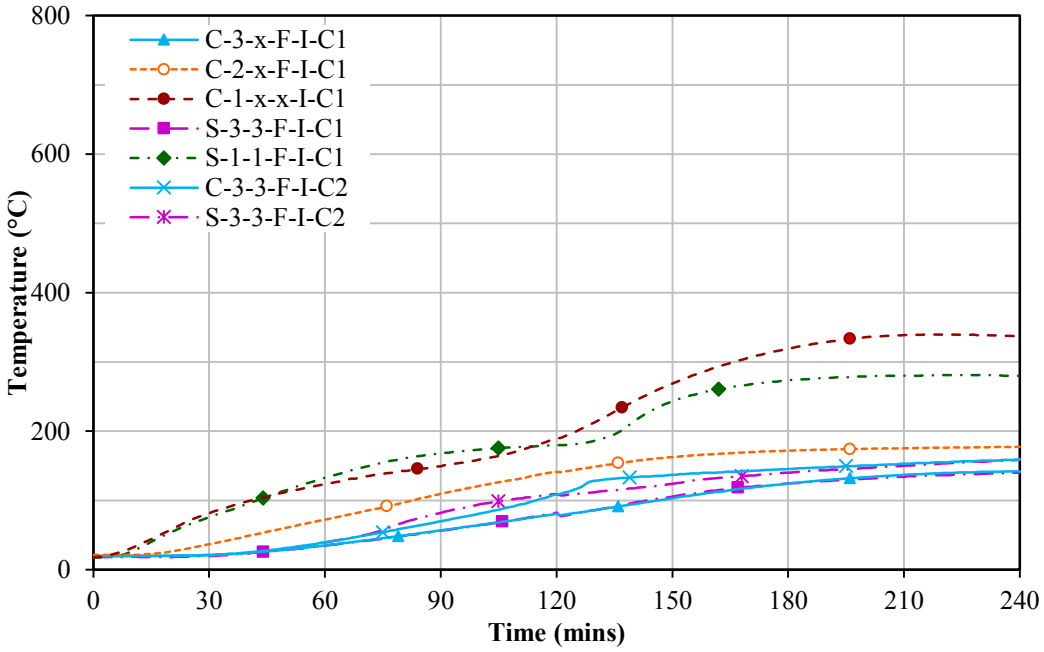

Figure 19: Observed average temperatures at the concrete centreline TCs for the protected tests

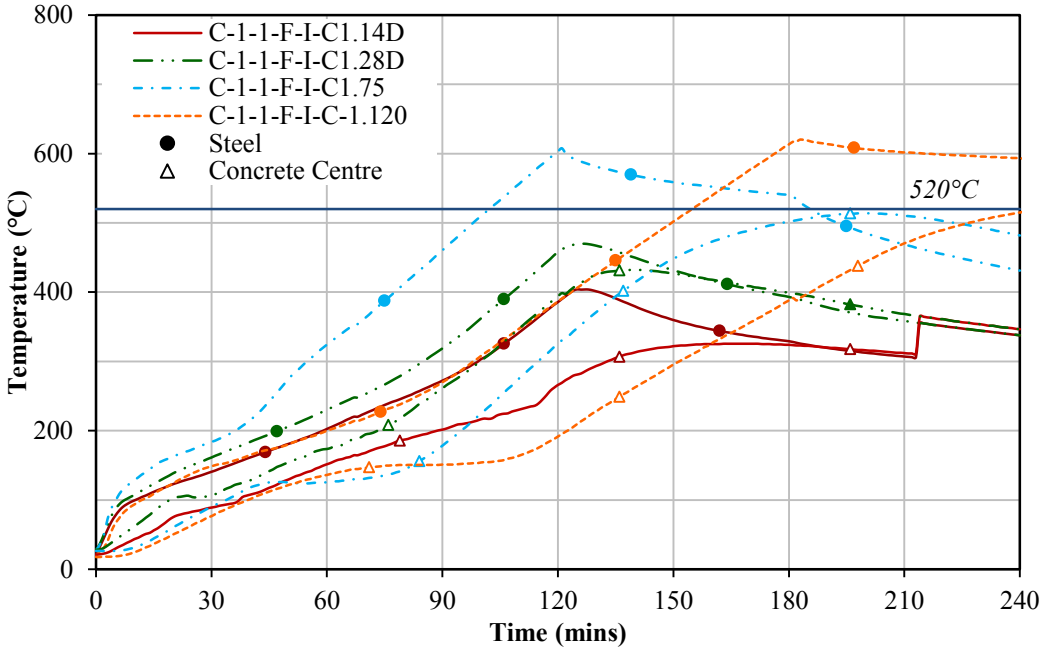

Figure 20: Observed average steel and concrete centre temperatures of the protected concrete age and protection thickness tests